12-1-2015

Glass shards at Pinnacle Point rock shelter 5-~6, South Africa: Are they from the last super-~eruption of Toba?

Amber Elizabeth Ciravolo
University of Nevada, Las Vegas, ciravolo@unlv.nevada.edu

GLASS SHARDS IN PINNACLE POINT ROCK SHELTER 5-6, SOUTH AFRICA: ARE THEY FROM THE LAST SUPER-ERUPTION OF TOBA?

By

Amber Ciravolo

Bachelor of Science – Earth and Environmental Science
Furman University
2012

A thesis submitted in partial fulfillment
of the requirements for the

Master of Science – Geoscience

Department of Geoscience
College of Sciences
The Graduate College

University of Nevada, Las Vegas
December 2015

UNLV | GRADUATE COLLEGE

Thesis Approval

The Graduate College
The University of Nevada, Las Vegas

November 13, 2015

This thesis prepared by

Amber Ciravolo

entitled

Glass Shards at Pinnacle Point Rock Shelter 5-6, South Africa: Are They from the Last Super-Eruption of Toba?

is approved in partial fulfillment of the requirements for the degree of

Master of Science – Geoscience
Department of Geosciences

Eugene Smith, Ph.D.
Examination Committee Chair

Kathryn Hausbeck Korgan, Ph.D.
Graduate College Interim Dean

Terry L. Spell, Ph.D.
Examination Committee Member

Minghua Ren, Ph.D.
Examination Committee Member

Chih-Hsiang Ho, Ph.D.
Graduate College Faculty Representative

ABSTRACT

Cryptotephra, in the form of individual glass shards, have been discovered in paleoarchaeological site PP5-6 North at Pinnacle Point, Western Cape, South Africa. This marks the first documentation of cryptotephra in a South African paleoarchaeological site. PP5-6 North is a rock shelter in the cliffs along the coast of the Western Cape and is one of a series of caves and rock shelters at Pinnacle Point that were inhabited by early modern humans. The presence of cryptotephra at PP5-6 is an important discovery in terms of tephra preservation in cave deposits as well as the possibility of tephra being present in other nearby locations. The cryptotephra at PP5-6 presented numerous challenges in terms of extraction and analysis. Shards were less than 60 micrometers in size and were extremely low in abundance. Electron probe analyses show that the shards are rhyolitic in composition and optically stimulated luminescence dating of the host sediment indicates the shards are 73.7 ka. This leads to the conclusion that the cryptotephra in PP5-6 may represent an ultra-distal deposit, more than 5000 km from the source eruption, of the 74 ka Toba super-eruption in Sumatra, Indonesia. The Toba caldera is 8964 km away from Pinnacle Point, making Pinnacle Point the most distal deposit of this eruption.

ACKNOWLEDGEMENTS

Thanks to all those who made this project a possibility. This project would have turned out vastly different if it had not been for everyone's help and advice. A special thanks to my adviser, Dr. Eugene Smith for advising me on the project and making multiple trips to South Africa to collect samples and study the geology around Pinnacle Point. This started as a small side project that Dr. Smith allowed me to work on that quickly grew to the time-consuming, multi-faceted project it is today. Thanks also to my committee members, Dr. Terry Spell, Dr. Minghua Ren, and Dr. Chih-Hsiang Ho, for enduring the change in thesis topics and the long wait until this thesis was completed.

The UNLV Tephra Lab would not have come into existence if not for the guidance of Dr. Christine Lane, now at the University of Manchester, and the group at Research Lab for Archaeology and the History of Art (RLAHA) at Oxford University. Dr. Lane taught me the basic procedure for cryptotephra extraction using the Blockley method and showed me how to set up a cryptotephra extraction lab. The lab would have taken much longer to create if not for Dr. Lane's guidance and advice.

EPMA analyses for this project were conducted at UNLV's EMiL Lab by Dr. Minghua Ren. Countless hours were spent looking for single shards and experimenting with beam conditions to ensure accurate data for the few shards we found as well as preparing new secondary standards from the MPI-Ding collection.

We would only have half of our current analyses if not for the assistance of Dr. Racheal Johnsen. She assisted in processing samples for shard identification and grinding slides for analysis. Her expert help led to the discovery of the pervasive and all-together nerve-wracking opaline problem. Thanks for that, Racheal. The opal is all yours. Many of the figures and tables in this thesis would not look nearly as nice as they do without her help and guidance in formatting and Illustrator wizardry.

This project was made possible by Dr. Curtis Marean, the site director at Pinnacle Point. When the initial shards were found, he asked Dr. Smith for help identifying and locating more. If not for his permission, we would never have been able to sample at Pinnacle Point or gotten to work with SACP4 group. He's endured three years of Dr. Smith and I coming to the site and digging tephra sampling grooves in previously perfect excavated sections.

This project was mainly supported by National Science Foundation grants BCS-1460366 to Eugene Smith (UNLV) and Curtis Marean (Arizona State University), a subcontract to UNLV from the Arizona State Institute of Human Origins, and another subcontract from supplemental funding to NSF grant BCS-0524087 to Curtis Marean. Minor funding at the start of the project was also provided by AAAS-PD through the Alan E. Leviton Student Research Grant Award as well as the Department of Geoscience at UNLV.

TABLE OF CONTENTS

LIST OF TABLES

LIST OF FIGURES

CHAPTER 1: INTRODUCTION

Tephra in the form of ash, on geological timescales, is deposited instantaneously after a volcanic eruption (Lowe, 2011; Branch et al., 2014) over a wide geographical area (Lane et al., 2014). This creates tephra layers of precise ages that are extremely useful for stratigraphic chronologies and for creating regional age frameworks that can link geological, paleoecological, paleoclimatic, and archaeological deposits (Lowe, 2011; Lowe et al., 2012; Lane et al., 2014). Tephra form visible stratigraphic markers that are thick within tens of kilometers of the source volcano (Lane et al., 2014) and thin out with increasing distance (Fisher and Schmincke, 1984). Thousands of kilometers from the source volcano, tephra may be deposited in layers too thin or too diffuse to be visible to the naked eye (Branch et al., 2014). These deposits are referred to as cryptotephra (crypto- meaning invisible), with individual shards typically less than 125 micrometers in length (Lowe, 2011; Lane et al., 2014). The greater extent of these cryptotephra deposits compared to visible deposits (Turney et al., 2004) greatly extends the application of tephra studies. Cryptotephra are interspersed within sediment and require the use of separation techniques to extract. Typical cryptotephra layers can range from tens to thousands of shards per gram in concentration (Lane et al., 2014).

In the past few years, processing and analytical techniques have improved to the point where extremely low abundance (ELA) cryptotephra, which are characterized by abundances of less than 10 shards/gram, have successfully been used to identify a source volcano and constrain the age of an archaeological deposit. One pioneering study of ELA cryptotephra was conducted by Housley et al. (2014) who used very small quantities of cryptotephra in windblown sand units at archaeological site Mirkowice 33 in northwest Poland to correlate them with the Glen Garry tephra from Iceland and determine the age of the deposits. Although the best environmental settings for preserving cryptotephra are lakes (Wulf et al., 2004; Pyne-O'Donnell, 2007), peat bogs (Pilcher et al., 1995; Wastegård et al., 2003), and marine sites (Housley et al., 2012), they can be found in a wide range of

environments, including aeolian and archaeological deposits (e.g., Balascio et al., 2011), which were previously not recognized as being conducive to cryptotephra preservation (Housley et al., 2014). However, archaeological sites have the added variable of high biological activity, which can facilitate migration, mainly downward, of material, including cryptotephra, causing incorrect placement of isochrons and creating false associations between the age of the tephra at the perceived isochron and an archaeological horizon (Housley et al., 2014).

Purpose and Goals

This thesis reports on the only tephrochronology study thus far conducted in a South African paleoarchaeological site in an attempt to determine if South Africa has cryptotephra usable for dating and correlating archaeological deposits. It investigates ELA cryptotephra found within Pinnacle Point rock shelter 5-6 North (PP5-6) in Western Cape Province, South Africa, with the purpose of identifying the source eruption of the cryptotephra using geochemical fingerprinting. The goals of this study were twofold: 1) to create a tephra laboratory at UNLV capable of efficiently extracting the ELA cryptotephra, and 2) to analyze the Pinnacle Point cryptotephra for major elements in order to successfully match it to a source eruption. The hypothesis is that the cryptotephra at PP5-6 represents a primary ultra-distal deposit of the 74 ka Youngest Toba Tuff (YTT) from the Toba caldera complex in Sumatra, Indonesia.

CHAPTER 2: BACKGROUND ON TEPHRA STUDIES

Tephra Studies in Africa

In Africa, tephra studies have been mainly conducted on visible late Miocene to early Pleistocene tephra horizons in eastern Africa in areas such as the Afar region, the Gulf of Aden, Lake Malawi, and the Turkana Basin (Figure 1; Brown et al., 1992; Haileab 1995; Feakins et al., 2007; Fontijn, 2010; Chorn, 2012). There are fewer studies focused on the Late Pleistocene (Blegen et al., 2015), which is the time period of interest in this thesis. One of these studies (Blegen et al., 2015) reports data on Late Pleistocene tephra in Lake Victoria and the surrounding area (Figure 1), creating the first regional record of tephra from the Late Pleistocene associated with archaeological deposits and fossils. The deposits documented by Blegen (2015) were visible layers. Studies focused on Late Pleistocene cryptotephra are even rarer (e.g., Lane et al., 2013, Barton et al., 2015).

An important cryptotephra study in eastern Africa (Chorn, 2012; Lane et al., 2013) resulted in the discovery of cryptotephra from the 74 ka YTT eruption in core from Lake Malawi (also called Lake Nyasa). Cores were taken from the lake sediment and both visible tephra and cryptotephra layers were discovered (Chorn, 2012). Tephra in some of the layers corresponded to eruptions from nearby volcanoes such as Rungwe (Figure 1), but one cryptotephra layer contained high-silica rhyolite shards that matched the major element chemistry of the YTT (Chorn, 2012; Lane et al., 2013). Earlier dating, based on both optically stimulated luminescence (OSL) and paleomagnetic studies for the core, reported the 74 ka age horizon nine meters below the layer containing the suspected YTT shards (Lane et al., 2013). The identification of YTT at Lake Malawi extended the known range of Toba tephra to over 7000 km from the source and reported the first documented discovery of the YTT in Africa (Chorn, 2012; Lane et al., 2013).

The volcanic activity in eastern Africa provides a great opportunity for creating a regional tephra framework, an opportunity that may also exist in northern and southern Africa, especially when cryptotephra studies are included. These areas would benefit greatly from additional tephrochronology studies because both northern and southern Africa have ample archaeological deposits containing evidence of early human habitation (Barton et al., 2015). However, archaeological sites in northern and southern Africa have only recently become the focus of tephra studies (e.g., Barton et al., 2015; this study), partially because of their relative lack of visible volcanic deposits compared to those in eastern Africa. Northern Africa, however, has recently been shown to have cryptotephra deposits from sources across the Mediterranean Sea (Barton et al., 2015). These cryptotephra deposits have been found in caves and rock shelters with some deposits containing thousands of shards per gram of sediment while others contain ELA cryptotephra (Barton et al., 2015) similar in abundance and size to the shards discovered at Pinnacle Point as part of this study.

Study and Dating of Cryptotephra in Archaeological Sites

Archaeological sites present a challenge to cryptotephra studies because they have been affected by human habitation (trampling, bioturbation, etc.) and are often located in caves and rock shelters where tephra accumulation is restricted. Open-air archaeological sites would have less restricted tephra accumulation but are more prone to disturbance (Lane et al., 2014). In the cave environment, deposition is usually indirect, meaning tephra is carried in by wind or water transport. It requires exceptional circumstances (e.g., large entrance or skylight, etc.) for cryptotephra to fall into the cave directly (Barton et al., 2015). However, caves and rock shelters may present some of the best opportunities for documenting cryptotephra sourced from widely dispersed eruptions if erosion and bioturbation effects are minimal (Barton et al., 2015).

Another challenge of completing a cryptotephra study is dating the tephra deposits. Both isotopic and relative dating techniques can be utilized to determine the age of tephra. Isotopic dating can be used on pyroclastic deposits using techniques such as $^{40}Ar/^{39}Ar$ (or K/Ar) on phenocrysts such as sanidine and biotite (Baadsgaard and Dodson, 1964; Lee et al., 2013), or on glass or groundmass if sufficient potassium is present. However, not all tephra deposits, especially those that are distal or ultra-distal, will have material of sufficient size or quantity for dating. Therefore, the applicability of the $^{40}Ar/^{39}Ar$ technique is limited for cryptotephra studies (Blockley et al., 2008; Lee et al., 2013). For cryptotephra deposits, indirect dating techniques such as OSL or radiocarbon dating that utilize material other than the tephra within the layer are more appropriate.

Figures

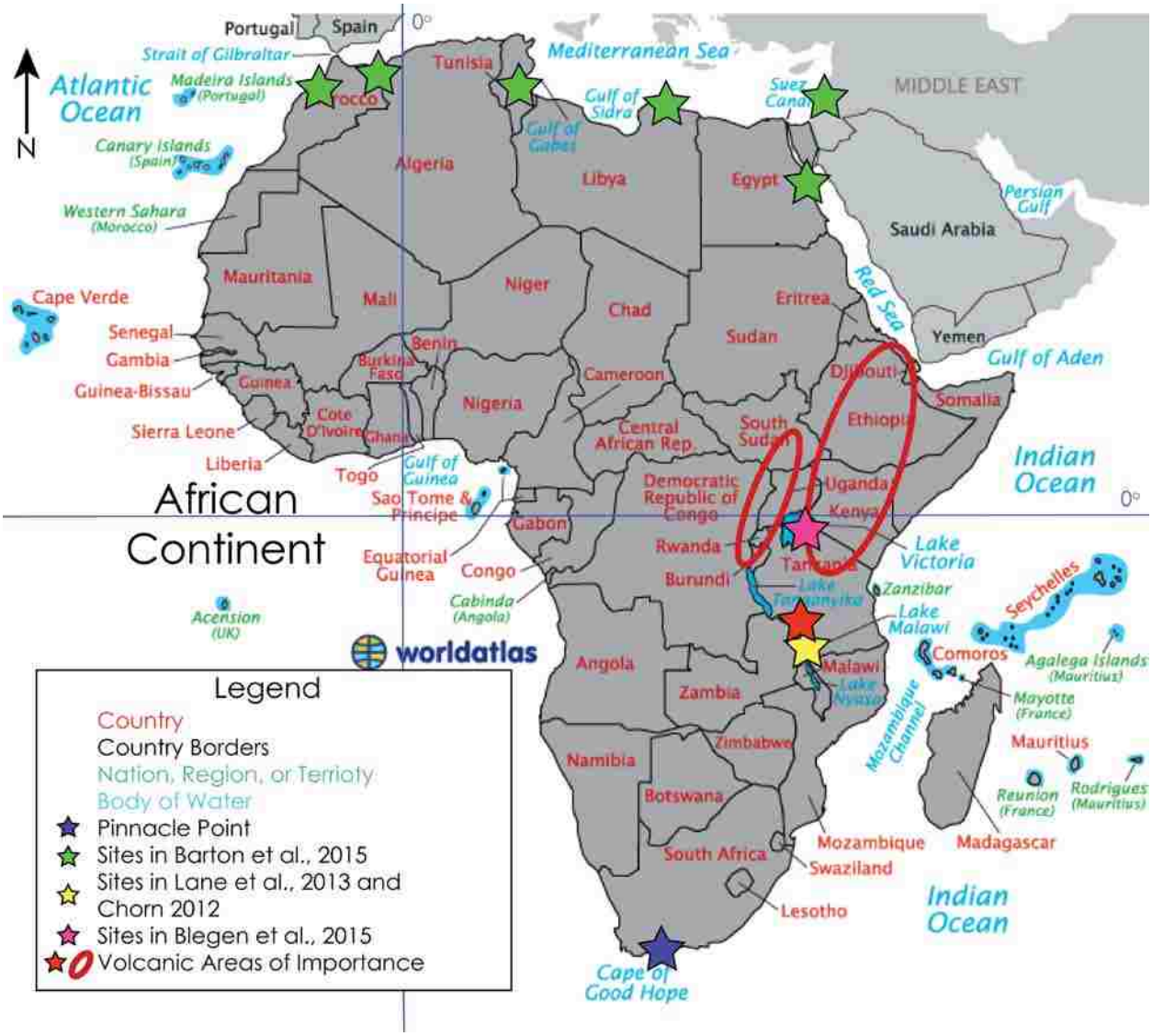

Figure 1: Map of relevant areas in Africa including sites of mentioned tephra studies, volcanic provinces, and Pinnacle Point. (Fontijn, 2010; Chorn, 2012; Lane et al., 2013; Barton et al., 2015; Blegen et al., 2015).

CHAPTER 3: BACKGROUND AND GEOLOGIC SETTING OF PINNACLE POINT

Background on Pinnacle Point

Pinnacle Point (Figure 2) is an area of coastal cliffs and shoreline 10 km west of Mossel Bay (Mosselbaai) in Western Cape Province, South Africa, that is replete with caves and rock shelters (Marean et al., 2010). The Pinnacle Point area sits on the convergence of the cold Benguela and warm Agulhas ocean currents (Bar-Matthews et al., 2010). It has year-round rainfall and is part of the Cape Floral Region, which boasts a diverse range of fauna and flora (Bar-Matthews et al., 2010; Marean et al., 2010). The generally temperate climate of the region may have made the area favorable to early modern humans (Henshilwood, 2008). Coastal South Africa contains the richest archaeological record for early modern human behavior (Bar-Matthews et al., 2010) and Pinnacle Point is one of the few areas in coastal Africa that has an archaeological record extending past 120 ka (Marean, 2010).

Above the cliffs where PP5-6 is located is a beach and golf resort that opened in 2006. In preparation for the construction of this resort, an environmental survey of the surrounding area was conducted in 1997 that resulted in the discovery of 28 archaeological sites, half of which were caves or rock shelters (Marean and Nilssen, 2002; Marean et al., 2004). Archaeological excavations at Pinnacle Point by Marean began in 2000 (Marean and Nilssen, 2002), with excavation at site PP5-6 beginning in 2006, as part of the South African Coastal Paleoclimate, Paleoenvironment, Paleoecology, Paleoanthropology (SACP4) project. The main goal of SACP4 is to link paleoclimate, paleoenvironmental, and paleoanthropological data from the South African southern coast (Brown et al., 2009; Oestmo and Marean, 2014). The goals of SACP4 are achieved by integrating studies from a wide range of disciplines including paleoclimatology, geology, archaeology, geochronology, and botany.

For this thesis, sampling for cryptotephra took place in PP5-6 North, a “slit-cut” rock shelter (Figure 2; Figure 4; Karkanas et al., 2015). PP5-6 South is another rock shelter connected to PP5-6, but to

date, no significant finds have been discovered in PP5-6 South, so PP5-6 North will be hereafter referred to as PP5-6. PP5-6 has late Middle Stone Age (MSA) archaeological deposits ranging in age from 90 to 50 ka as dated by the OSL technique (Smith et al., in prep). These deposits are important because they fill a gap in the archaeological record for the area. Most of the other Pinnacle Point sites lack sediments younger than 90 ka because sand dunes blocked the entrances of many of the caves at Pinnacle Point at this time, preventing human habitation and further accumulation of a sedimentary section (Marean et al., 2007; Bar-Matthews et al., 2010). PP5-6 contains hearths, stone tools (lithics), marine shells, ostrich egg shells, and animal bones (Brown et al., 2009).

Geologic Setting of Pinnacle Point

The cliffs at Pinnacle Point are composed of Ordovician Skurweberg Quartzite (Marean and Nilssen, 2002), which is part of the Table Mountain Group (TMG), a member of the Cape Supergroup (Figure 3; Keyser, 1997). The quartzite was folded and faulted during the Permo-Triassic orogenic event that formed the Cape Fold Belt (Bar-Matthews et al., 2010). Fault breccias were formed along shear zones and faults during this event (Bar-Matthews et al., 2010). The caves and rock shelters at Pinnacle Point formed by erosion of these fault breccias (Marean et al., 2004; Bar-Matthews et al., 2010; Marean et al., 2010), primarily during sea level high stands (Karkanas and Goldberg, 2010; Karkanas et al., 2015).

The quartzite at PP5-6 is coarse-grained and light gray in color and is capped by calcrete and dunes (Marean and Nilssen, 2002; d'Errico and Henshilwood, 2007; Bar-Matthews et al., 2010). Numerous quartz veins and nodules run through the quartzite. The calcrete capping the quartzite is variable in thickness from over a meter to just a thin veneer (Marean and Nilssen, 2002). This calcrete at Pinnacle Point is important to the archaeology of the area because it buffers the pH of water that enters the caves and rock shelters (Bar-Matthews et al., 2010) making conditions favorable for bone preservation (Marean and Nilssen, 2002).

Field Description of PP5-6

PP5-6 contains several archaeological deposits. These are the South Remnant, Northwest Remnant, and the Long Section (Figure 4; Karkanas et al., 2015). The Long Section holds the majority of excavated archaeological material and has been the focus of archaeological work as well as the location where the cryptotephra samples were collected. Because of these factors, the Long Section is the only deposit described in detail here.

The Long Section is a nearly continuous sedimentary section that is 30 meters long, 14 meters of which have been excavated (Karkanas et al., 2015). The Long Section is divided into eight units called Stratigraphic Aggregates (Figure 4). The Stratigraphic Aggregates in the Long Section include, from youngest to oldest: Reddish Brown Sand and Roofspall (RBSR), Black Compact Sand and Roofspall (BCSR), Dark Brown Compact Sand (DBCS), Orange Brown Sand 2 (OBS 2), Shelly Gray Sand (SGS), (OBS 1), Shelly Ashy Dark Brown Sand (SADBS), Ashy Light Brown Sand (ALBS), Light Brown Sand and Roofspall (LBSR), Yellowish Brown Sand and Roofspall (YBSR), and Yellowish Brown Sand (YBS) (Figure 4; Karkanas et al., 2015, Brown et al., 2012). These Stratigraphic Aggregates are subdivided into subunits known as sub-aggregates.

Panagiotis Karkanas, micromorphologist at the American School for Classical Studies, initially discovered shards in an impregnated thin section of the SADBS stratigraphic aggregate. As a result of his findings, sampling of SADBS and the ALBS stratigraphic aggregates was the focus of this thesis. Sampling of the OBS1, above the SADBS, and LBSR, below the ALBS, was conducted in subsequent years and are the focus of future work.

The SADBS was the uppermost stratigraphic aggregate sampled for this thesis. It is about 70 cm thick (Brown et al., 2012) and has a weighted mean OSL age of 71 ± 3 ka (Karkanas et al., 2015). The sub-aggregates sampled for this study were, from top to bottom: Kim, Enrico, Gert, Sydney, Thandesiswe,

Erich, and Jocelyn (Figure 7). The SADBS consists of dark brown aeolian sand, roofspall (quartzite from the walls of the rock shelter), and ash from the burning of wood and other plant material (Karkanas et al., 2015; Brown et al., 2012). Large portions of the SADBS are concreted and were difficult to excavate and sample. Hammers were often used to facilitate the removal of the concreted areas. The SADBS is rich in marine shell material, and contains fire-modified rock, ochre, lithic fragments, ostrich egg shell fragments, and animal teeth and bones (Brown et al., 2009). A major discovery made during excavation is the presence of an advanced lithic technology that is dominated by microliths (small bladelets) created from silcrete (a cemented crust formed by silica accumulation (Nash et al., 2013) first described by Lamplugh (1902)) that was processed using heat (Brown et al., 2012). The use of heat treaded silcrete represents a major advance in human technology because earlier lithic fragments were primarily quartzite with minor amounts of unprocessed silcrete, chert, and chalcedony (Brown et al., 2009).

The ALBS is 76 cm thick and lies directly beneath the SADBS (Figure 4; Brown et al., 2012). The contact between SADBS and ALBS is planar and fairly distinct (Brown et al., 2012). The ALBS has a weighted OSL mean age of 72 ± 3 ka (Karkanas et al., 2015). The sub-aggregates of the ALBS sampled for this study were Conrad Sand and Conrad Cobble and Sand (Figure 7). The ALBS is mainly composed of yellow aeolian sand as well as fine gray ashy material (Brown et al., 2009). The ALBS is poorly consolidated sand that tends to slump during sampling and is relatively barren of archaeological artifacts compared to the overlying SADBS (Marean, personal communication 2014). Finds include marine shells, animal bones and teeth, lithics, and ostrich eggshell fragments (Brown et al., 2009).

Field sampling

The methods used in this study for sampling are similar to those commonly used in tephrochronology for extracting cryptotephra (e.g., Lane et al., 2014). Typically, samples are collected every centimeter or every few centimeters from bottom to top, creating a small groove in the vertical

transect of the sample area. However, for this thesis, samples were collected from top to bottom to minimize active slumping and contamination.

Dr. Eugene Smith and Deborah Keenan collected the materials used for this study in the SADBS and ALBS stratigraphic aggregates during the southern hemisphere winter 2012 field season (Figure 5). They collected 130 samples in two transects approximately one meter apart. Transect 1 contained samples PP-612-1 through PP-612-88 and transect 2, samples PP-612-89 through PP-612-130. Sample locations in conjunction with subaggregate information can be found in Appendix B. The two sample profiles covered approximately the same portions of the stratigraphic sections. Subsequent sampling was conducted in 2013 by Dr. Curtis Marean in the OBS1, the unit directly above the SADBS (Figure 4), and in 2014 by Amber Ciravolo in the LBSR and ALBS below and approximately one meter west of the initial samples collected by Smith and Keenan.

All areas used for sampling were first brushed or scraped of any foreign material. This was necessary because the area was the site of a previous excavation and had subsequently been covered with sand bags. After cleaning the profile during the 2012 field season, Smith and Keenan collected several grams of sample every centimeter from the top of the section to the bottom. Nalgene bottles were used in 2012 to store the samples. After a sample was collected, the coordinates were recorded using a total station laser controlled GPS unit that provides millimeter accuracy (Dibble et al., 2007; Brown et al., 2012). This location data was uploaded into an ArcGIS 10.3 geodatabase that includes data for archaeological artifacts, OSL dating sampling sites, and stratigraphic position within the Stratigraphic Aggregate (Brown et al., 2012). At the end of the field season, photo chits were placed around the collection area and a GPS-rectified photo was taken of the sample location. Details of the archaeological excavation methods employed at Pinnacle Point are described elsewhere (Marean et al., 2004; Dibble et al., 2007; Marean et al., 2010; Bernatchez and Marean, 2011) as are micromorphology methods (Karkanas and Goldberg, 2010; Karkanas et al., 2015).

Figures

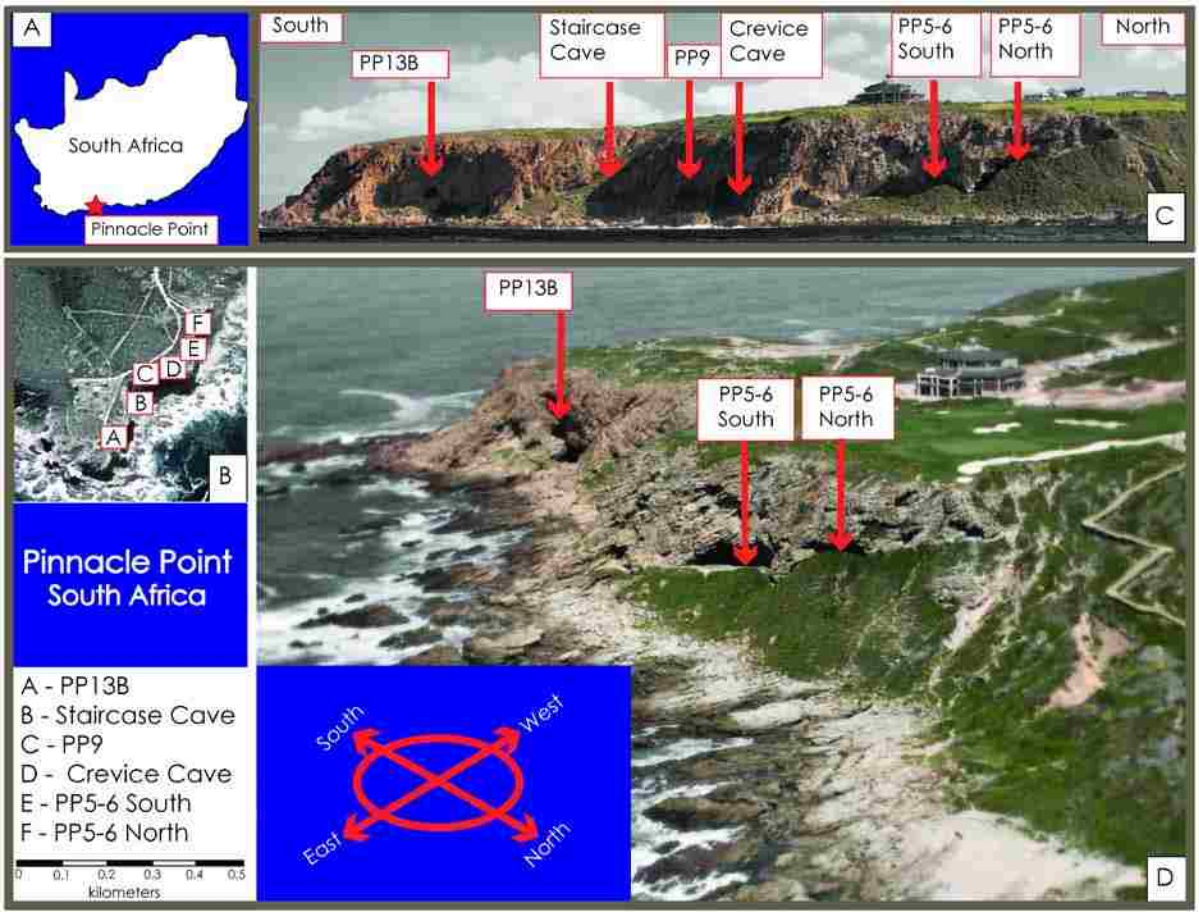

Figure 2: A. Location of Pinnacle Point on the coast of Western Cape, South Africa. B. Aerial view of several caves and rock shelters at Pinnacle Point. C. View of Pinnacle Point caves and rock shelters. D. Pinnacle Point 5-6 North and South (modified from Karkanas et al., 2015).

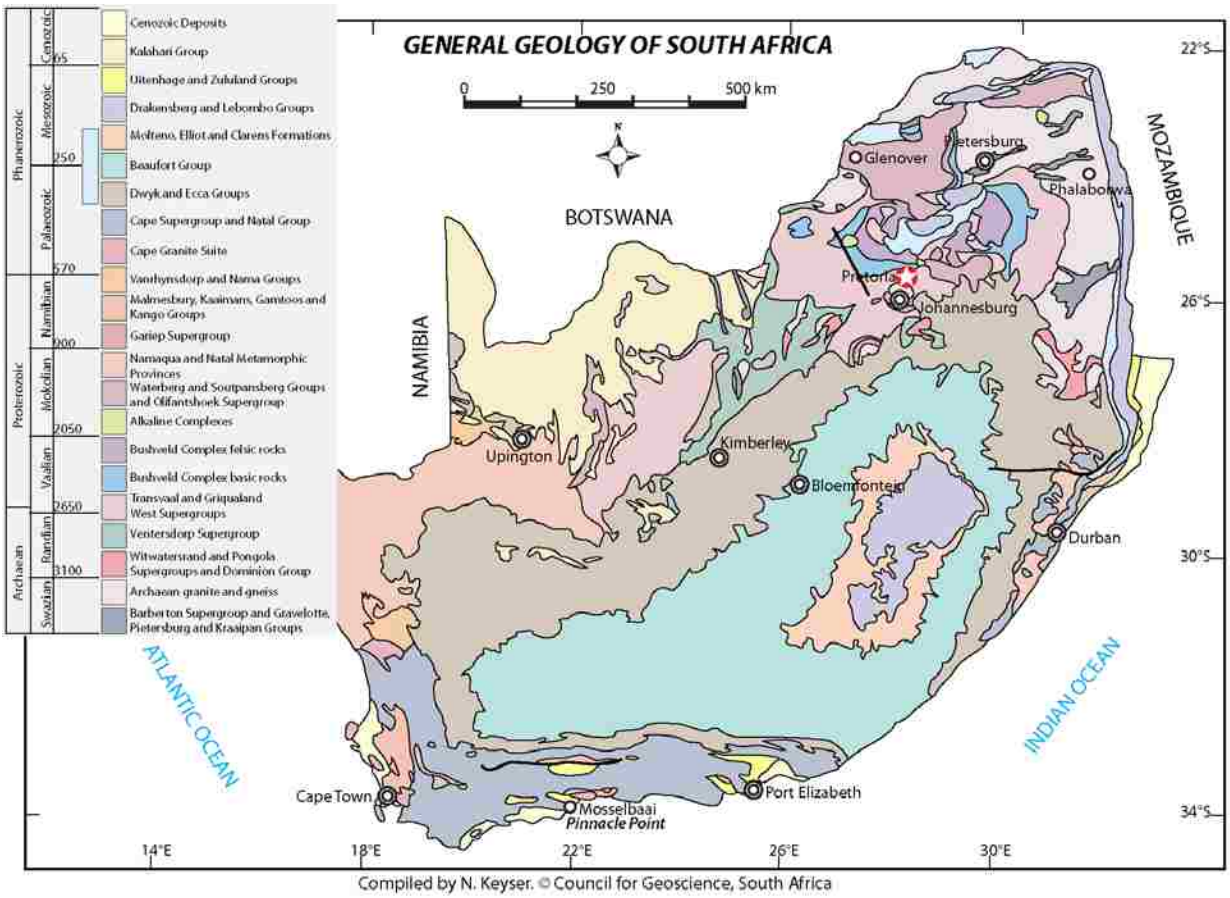

Figure 3: Generalized geologic map of South Africa. The dark blue represents the Cape Supergroup and Natal Group which includes the Table Mountain quartzite found at PP5-6. Map modified from Keyser (1997).

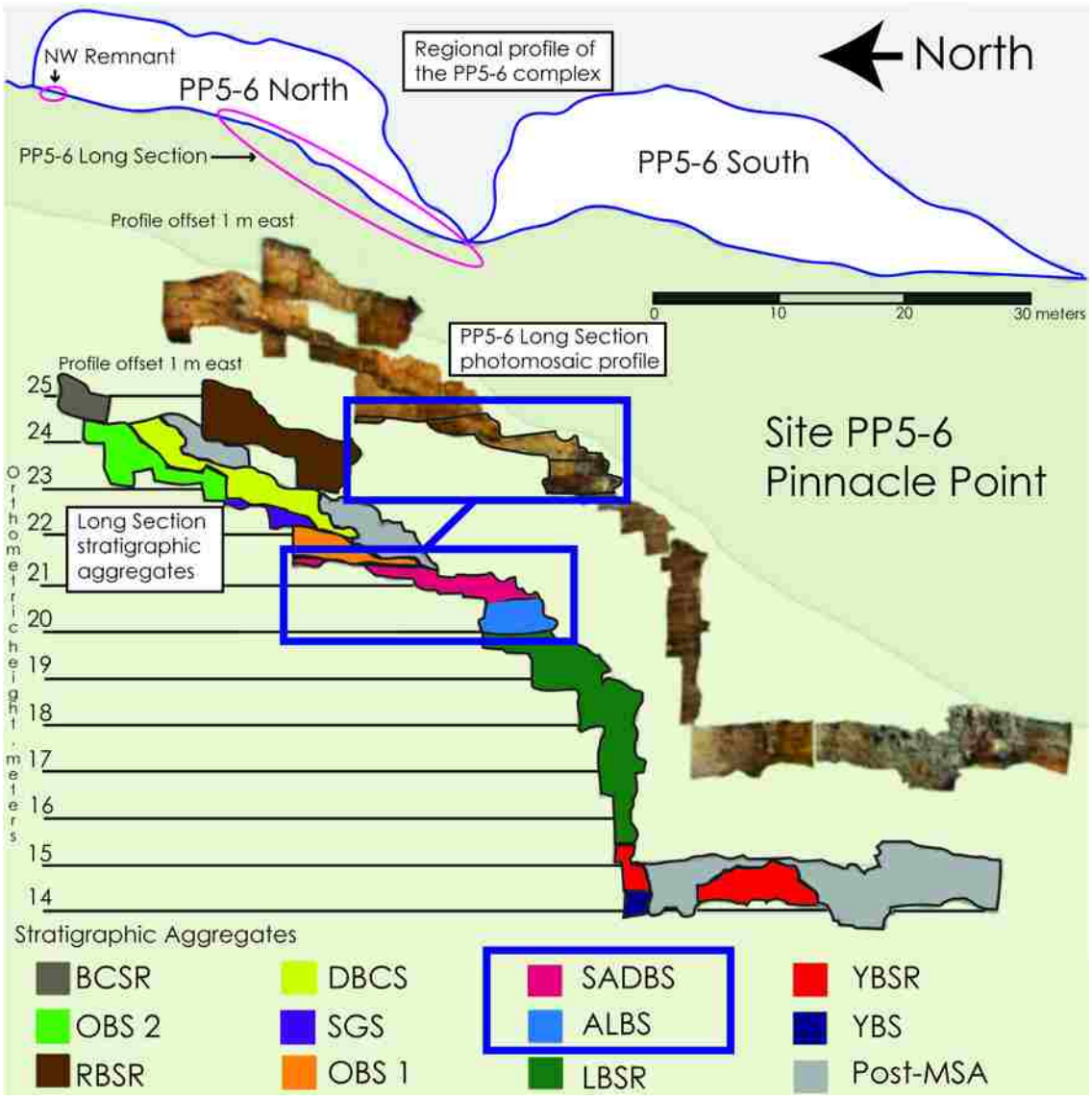

Figure 4: Stratigraphy of archaeological deposits in PP5-6. The dark blue rectangles show the Stratigraphic Aggregates sampled for cryptotephra in this study. (Figure modified from Karkanas et al., 2015).

Figure 5: Photograph of a sample groove cut while collecting sediment samples in 2012.

CHAPTER 4: LAB SETUP AND METHODS

The first goal of this study was to create a lab at UNLV that specialized in the processing of ELA cryptotephra, which included modifying existing cryptotephra extraction techniques for ELA cryptotephra. Cryptotephra processing, in general, is a meticulous and laborious process that typically includes acid digestion, and density and/or magnetic separation procedures to extract the cryptotephra from its host sediment (Gehrels et al., 2008). The size and abundance of the shards at PP5-6 were unknown at the start of this study, and the expertise to process cryptotephra was not at that time present at UNLV. The Electron Microscopy Lab at the University of Utah was contacted and Drs. Frank Brown and Scott Hynek, the laboratory director and research associate, respectively, agreed to process a test sample. Processing took over six months and analysis at Utah was not successful at locating shards due to the presence of numerous very large quartz and feldspar grains. This attempt illustrated the problems of using standard tephra processing techniques when dealing with cryptotephra, particularly ELA cryptotephra.

While waiting for results from Utah, unprocessed grain mounts of sample PP-612-97 were made on petrographic slides that were polished and scanned for shards using the Scanning Electron Microscope (SEM) at UNLV. This method was extremely time intensive, but one 60 micrometer rhyolite shard was discovered (97-shard-A). Unfortunately, the shard was lost during polishing after a preliminary Electron Probe Microanalyzer (EPMA) analysis. When the Utah lab returned the test sample, scanning the slide using SEM Energy Dispersive Spectroscopy (EDS) yielded another 40 micrometer rhyolite shard (GS335). This initial work indicated that the shards were likely small overall and not very abundant.

Because of the small size and scarcity of shards, the new UNLV lab adopted a modified version of the cryptotephra flotation extraction procedure of Blockley et al. (2005). Flotation extraction for cryptotephra was first introduced in the 1990s (Turney et al., 2004). The Blockley et al. (2005) technique

was chosen because it avoids processes that could potentially cause chemical alteration of the shards. Other techniques such as ashing, the combustion of organic material, and heavy chemical digestion, which are used to extract cryptotephra from organic-rich sediments (Dugmore, 1989; Pilcher and Hall 1992), have not been widely successful in extracting cryptotephra from aeolian and other deposits rich in quartz and other inorganic silicic material (Turney et al., 2004). These techniques also have the potential to alter the chemistry of the shards (Dugmore et al., 1992; Gehrels et al., 2008). Heavy liquid separation techniques, such as those employed by Blockley et al. (2005), are more time consuming and are only particularly useful when extracting silica-rich cryptotephra (Gehrels et al., 2008). In July-August 2013, Ciravolo traveled to Oxford University to study the setup of the cryptotephra lab at the Research Laboratory for Archaeology and the History of Art (RLAHA) and learn, under the guidance of Dr. Christine Lane, the extraction procedure outlined in Blockley et al. (2005). During this time, 20 samples from Pinnacle Point were processed. Using the techniques learned in the Oxford lab, a similar tephra lab was established at UNLV during the fall semester of 2013. All materials and equipment used to set up and maintain the UNLV lab are documented in Appendix A (Table A2). Figure 6 shows a schematic flow chart of the basic procedure. Essential materials include sieves, a centrifuge capable of running at 2500 rpm, and a heavy liquid such as Sodium Polytungstate (SPT; standard density of 2.82 g/cm^3) or Lithium Metatungstate (LMT; standard density of 2.95 g/cm^3).

There are several differences between the Oxford and UNLV labs in both equipment and procedure (Table 1). The main differences relate to modifications in procedure made at the UNLV lab to specifically deal with ELA cryptotephra. The minimum sieve mesh was lowered because a smaller grain size was expected due to the distal nature of the site, which is approximately 3000 km from the nearest Pleistocene volcano. Epoxy was used (Epothin) as the mounting agent for the reference slides instead of Canada Balsam. This increased drying time for the slides and introduced the possibility that slides might become unusable due to improper curing; however, any shards found on these reference slides could be

polished for EPMA analysis. The double use of the reference slides for both shard counting and geochemical analysis eliminated the need for using a micromanipulator to extract shards. Because using the micromanipulator is both labor- and time-intensive, eliminating the need for the manipulator decreased sample processing time significantly. Another difference was using LMT rather than SPT, but LMT and SPT heavy liquids are interchangeable so this difference did not affect the procedure. Both heavy liquids are nontoxic but cannot be used at densities as high as those attained by methylene iodide (MI), which has a density of 3.33 g/cm^3. MI is used to separate heavy minerals such as zircon and requires a fume hood. By using one of the nontoxic heavy liquids, separations can be done without the use of a fume hood.

Processing and Identification of Cryptotephra

Samples were weighed to approximately one gram and placed in 50 mL centrifuge tubes. A 10% solution of hydrochloric acid was used to dissolve the carbonates. The samples were subsequently sieved at 80 and 20 μm, keeping the 20-80 μm portion. The 20-80 μm sieve portion was further processed using LMT at densities of 1.95 g/cm^3 and 2.55 g/cm^3 to separate the glass shards and other low-density grains. Samples were centrifuged twice at each density for 15 minutes at 2500 rpm. After cleaning, the separate containing shards (1.95 – 2.55 g/cm^3) was mounted on petrographic slides using Epothin epoxy. The slides were scanned to count the shards using a petrographic microscope fitted with a mechanical stage. This count is reported as shards per gram of dried sediment (s/g) and plotted against vertical position in the sediment column to construct a shard frequency diagram (Figure 7). Slides with identified shards were ground and polished for geochemical analysis. A complete description of techniques is provided in the lab manual in Appendix A.

Cryptotephra Analytical Methods

The Pinnacle Point shards were very sparse and small and, hence, difficult to analyze. All shards were less than 60 μm in diameter. Polished analytical surfaces were usually much smaller and grinding

and polishing the slides for single grains was labor- and time-intensive. Because of these difficulties, good analyses with wt. % totals above 93 wt. % have only been obtained for three shards, in samples 48, 49, and 125.

The shards were analyzed for major and minor elements using a JEOL JXA-8900 SuperProbe EPMA with four wavelength dispersive spectrometers (WDS). EPMA WDS was chosen because the instrumental parameters such as counting time can be strictly controlled and monitored for each element (Branch et al., 2014). Because of low abundance, techniques such as X-ray fluorescence spectrometry (XRF) would not be viable for ELA cryptotephra (e.g., Chorn, 2012). Optimal analytical conditions for EPMA were 10 nA current at 15 kV accelerating voltage using a 10 µm spot size (Lane et al., 2014), but experiments were conducted by varying beam current and beam diameter (Appendix C). Peak and background counting times were 30 sec and 10 sec, respectively. Peak and background counting times for Na were 10 sec and 5 sec. Alkali elements Na and K were counted on the first WDS cycle to minimize potential element migration from beam damage. The rhyolite glass standard ATHO-G, a part of the MPI-DING international standard set 1, was used as an internal standard for analyses (Table 2, Jochum et al., 2006). This standard was chosen for correlation with work done by Christine Lane at Lake Malawi (Chorn, 2012; Lane et al., 2013). Earlier analyses used NMNH 2231 synthetic tektite glass and VG-568 rhyolite glass standards from the Smithsonian and Harvard collections (Table 2, Jarosewich et al., 1980a; Jarosewich et al., 1980b).

Tables

Table 1: Differences between the Oxford and UNLV labs.

	UNLV Lab	Oxford Lab
Heavy Liquid	Lithium Metatungstate	Sodium Polytungstate
Method	Increased cleaning phases	Final sieve phase after cleaning
Centrifuge type	Ample Scientific Champion S50 D centrifuge	Jouan C 412 centrifuge
Centrifuge Capacity	8 spaces in centrifuge for 15 mL tubes	20+ spaces in centrifuge for 15 mL tubes
Slides	Mounted in epoxy	Mounted in Canada Balsam
Sieve Mesh	20 micrometer sieve mesh	25 micrometer sieve mesh
Analysis	Polished reference slides	Hand-picked shards using micromanipulator

Table 2: ATHO-G Standard analysis average and one standard deviation

	ATHO-G	ATHO-G Average (n=67)	ATHO-G Standard Deviation	VG568	VG568 Average (n=47)	VG568 Standard Deviation	NMNH 2231	NMNH 2231 Average (n=50)	NMNH 2231 Standard Deviation
SiO2	75.90	75.49	0.52	76.71	76.30	0.49	75.75	75.11	0.39
TiO2	0.24	0.24	0.04	0.12	0.07	0.02	0.50	0.49	0.02
Al2O3	12.00	12.27	0.25	12.06	11.98	0.16	11.34	11.01	0.12
Cr2O3		0.02	0.05		0	0.01		0.01	0.01
FeO	3.13	3.22	0.11	1.28	1.1	0.05	4.96	4.86	0.07
MnO	0.10	0.10	0.03	0.03	0.03	0.01	0.11	0.11	0.02
MgO	0.17	0.09	0.02	0.10	0.03	0.02	1.51	1.41	0.05
CaO	1.67	1.63	0.09	0.50	0.43	0.02	2.66	2.62	0.06
Na2O	4.31	4.26	0.19	3.75	3.74	0.25	1.06	0.97	0.1
K2O	2.65	2.69	0.2	4.89	4.97	0.12	1.88	1.85	0.07
P2O5	0.03	0.02	0.03	0.01	0.01	0.02		0.02	0.02
F		0.08	0.12		0.18	0.19		0.07	0.11
Cl		0.04	0.03		0.11	0.01		0.01	0.02
Total	100.20	100.16		99.45	98.87		99.77	98.52	

Figures

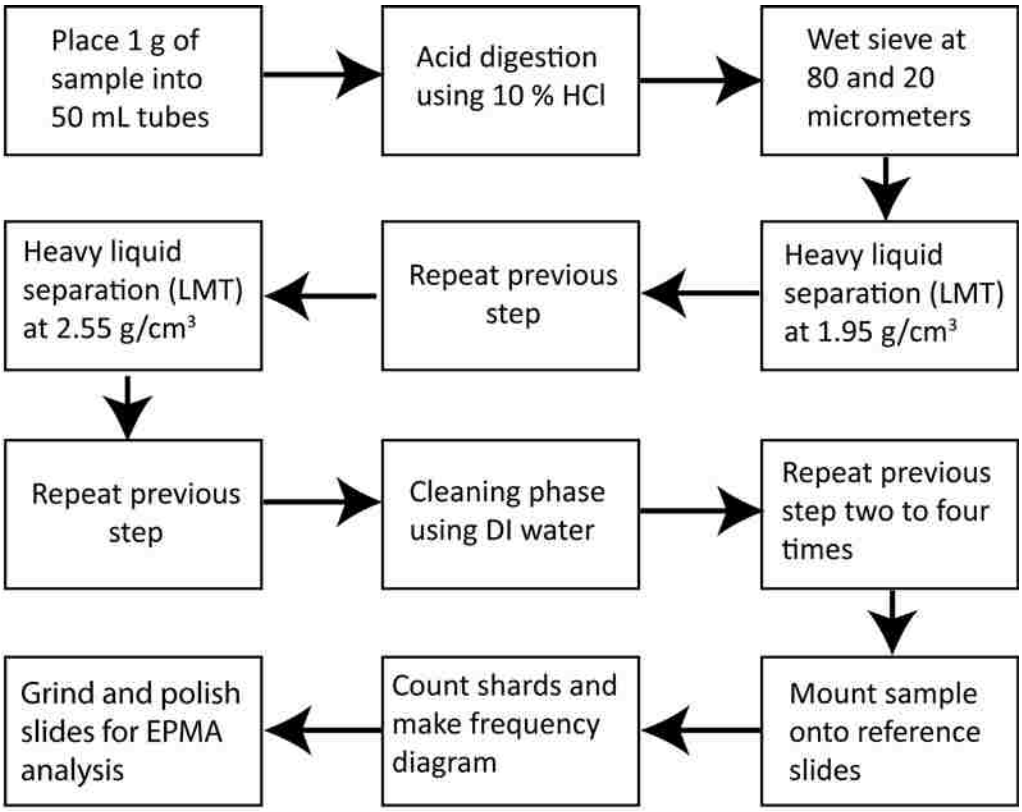

Figure 6: Schematic flow diagram for the processing of cryptotephra in the UNLV lab.

CHAPTER 5: RESULTS

Shard Profile at PP5-6

Figure 7 shows the distribution of the shards in the SADBS and ALBS stratigraphic aggregates. Reported are values for two vertical transects. Each bar represents a sample collected and scanned for shards. A list of sample numbers with corresponding sub-aggregates is included in Appendix B (Figure B1). The first appearance of shards occurs near the base of the Conrad Sand in the ALBS (Figure 7). Maximum shard abundance is three shards per gram of sediment. Gaps in shard abundance occur in the Conrad Sand/Jocelyn, Thandesizwe, and Enrico (Figure 7). Peaks of maximum shard abundance occur in Conrad Sand, Jocelyn, Erich, and Gert sub-aggregates (Figure 7). EPMA analyses were obtained from two shards in the Erich sub-aggregate, one in the Conrad Sand sub-aggregate, and one in the Sydney sub-aggregate (Figure 7).

Shard Morphology

Glass shards can come in a variety of different morphologies from vesicular to platy or bubble-wall. Color can vary from brown to colorless depending on the composition. The Pinnacle Point shards generally have blocky or bubble wall shapes, are clear in color, and generally lack vesicles. All shards are phenocryst-free and are less than 60 micrometers in size. Figure 8 shows the morphology of the shards found to date.

In Figure 8A, two possible shards are shown from a large format thin section composed of sediment from the SADBS. The shard to the left contains multiple vesicles. Both appear to be bubble-wall shards with cuspate margins and irregular shapes, similar to shard GS335 in Figure 8B. The shards shown in Figure 8A were discovered by Panagiotis Karkanas (personal communication, 2012). GS335, shown in Figure 8B is from sample PP-612-48 in the ALBS. It is 40 micrometers in length, has bubble-wall morphology with several cuspate margins separated by a thin septum, and has one vesicle in the upper

portion. Shard 97-Shard-A (Figure 8C.), from sample PP-612-97 in the Sydney sub-aggregate of the SADBS, has cuspate margins and lacks vesicles. Shard 125 (Figure 8D.), located in the sub-aggregate Conrad Sands in the ALBS, is platy and lacks vesicles. Similarly, shard 49 (Figure 8E), located in the sub-aggregate Erich in the upper ALBS, is platy with no vesicles.

Pinnacle Point Shard Discussion

The small size of the PP5-6 shards indicates that PP5-6 contains a distal or ultra-distal deposit (over 5000 km from the source). In general, larger particles fall out closer to the source; the more distal the deposit, the thinner the deposit, and the smaller the average shard diameter (Pyle, 1989; Fisher and Schmincke, 1984). The size and abundance of phenocrysts also decreases with distance from the source volcano. The quantity of shards (<10 shards/gram) indicates that, as well as being a distal or ultra-distal site, the depositional environment was not ideal for tephra deposition. For example: shards are thought to enter caves and rock shelters with their host sediment and are rarely deposited directly into the cave/rock shelter except in especially favorable conditions (Barton et al., 2015).

Shard Chemistry

Four shards have been analyzed to date by EPMA, shown in images B-E in Figure 8. Stars in Figure 7 denote their locations. The first two shards found at UNLV, 97-Shard-A and GS335, were first analyzed using SEM EDS. After identification by SEM EDS, the shards were analyzed by EPMA. All subsequent shards were found using a petrographic microscope and then analyzed by EPMA. Raw data are reported in Table 3. The data are plotted in Figures 9 and 10. Only analyses with totals above 94 wt. % were included in the results. However, 97-shard-A was included in Table 3 as a comparison for normalized data in subsequent figures. All other analyses are reported in Appendix C. Multiple major element analyses were obtained for shards 125 and 49 but only one for 97-Shard-A. GS335 had multiple analyses, but only two had a total greater than 94 wt. %. The Pinnacle Point shard analyses plot in the

rhyolite field on a total alkalis versus SiO_2 diagram (Figure 9; LeBas et al., 1986) when analyses are normalized to 100 wt. %.

Shards 125 and 49 have between 75 and 78 wt. % SiO_2 and 12-13 wt. % Al_2O_3 (Figure 10A). Shard GS335 has SiO_2 contents ranging from 71 to 72 wt. %, which is lower than the other shards, while its Al_2O_3 content is 15 to 16 wt. %, two to three wt. % higher than the other Pinnacle Point shards (Figure 10A). All of the shards have CaO between 0.7 and 0.9 wt. % (Figure 10B). Na_2O for GS335 is between 4 and 5 wt. %, slightly higher than the other shards (Figure 10C). Two analyses for shard 49 have Na_2O concentrations between 1-3 wt. % while the other analyses of shard 49 and shard 125 have between 3 and 4 wt. % Na_2O. GS335 shows a range of K_2O while all other shards have K_2O between 5 and 6.5 wt. % (Figure 10D). FeO for shard 125 is less than 1 wt. %, while FeO for GS335 is between 1 and 2 wt. % (Figure 10E). For MgO, GS335 is between 1 and 2 wt. % (Figure 10F). All other Pinnacle Point shards have MgO values under 1 wt. %. MnO content varies between 0.3 and 0.11 wt. % (Figure 10G) but shard 125 has higher MnO than the other shards. TiO_2 in GS335 is between 0.2 and 0.3 wt. %; the highest of the Pinnacle Point shards (Figure 10H). Shards 49 and 125 have between 0 and 0.2 wt. % TiO_2 (Figure 10H).

Tables

Table 3: Major element EPMA analyses in wt. % for the Pinnacle Point shards.

Sample	SiO_2	Al_2O_3	FeO	MgO	MnO	CaO	Na_2O	K_2O	TiO_2	Total
125	72.89	12.66	0.76	0.02	0	0.7	3.14	4.97	0	95.14
125	72.6	12.73	0.78	0.02	0.07	0.74	3.48	5.14	0	95.56
125	71.72	11.92	0.8	0.04	0.1	0.74	3.23	5.18	0.11	93.84
GS335	69.00	15.22	1.23	0.15	0.05	0.65	4.01	5.94	0.29	96.53
GS335	69.33	14.85	1.3	0.15	0.06	0.73	4.14	5.16	0.22	95.94
49	73.41	11.5	1.33	0.06	0.03	0.69	2.97	5.78	0.17	95.94
49	73.35	11.39	1.46	0.06	0.03	0.67	1.82	5.40	0.15	94.33
49	73.41	11.82	1.55	0.04	0.05	0.73	2.81	5.38	0.17	95.96
97	40.65	6.81	0.15	0.03	0.04	0.44	1.21	2.52	0.02	51.87

Figures

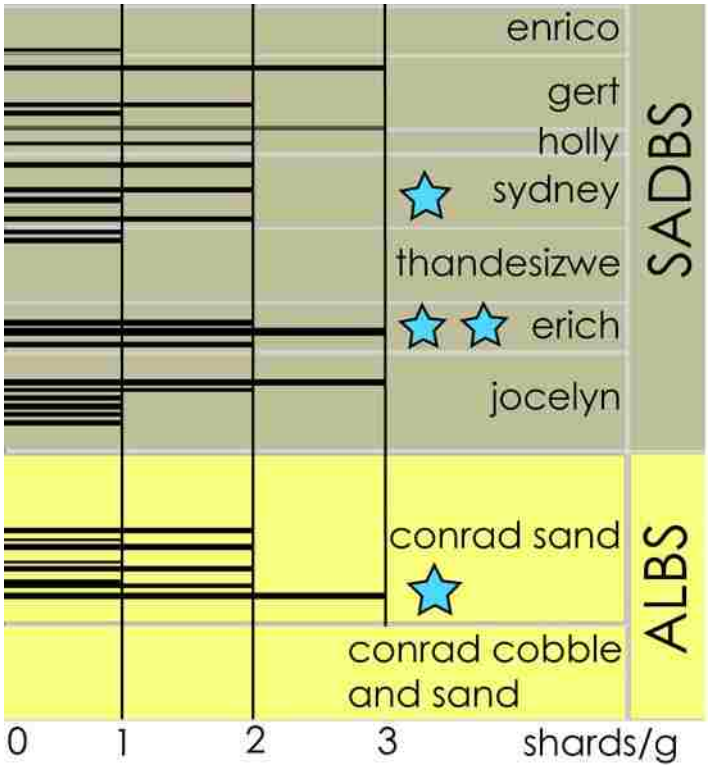

Figure 7: Shard distribution profile reported in shards/gram of loose material (Smith et al., in prep). Blue stars indicate sub-aggregates where EPMA analyses were conducted.

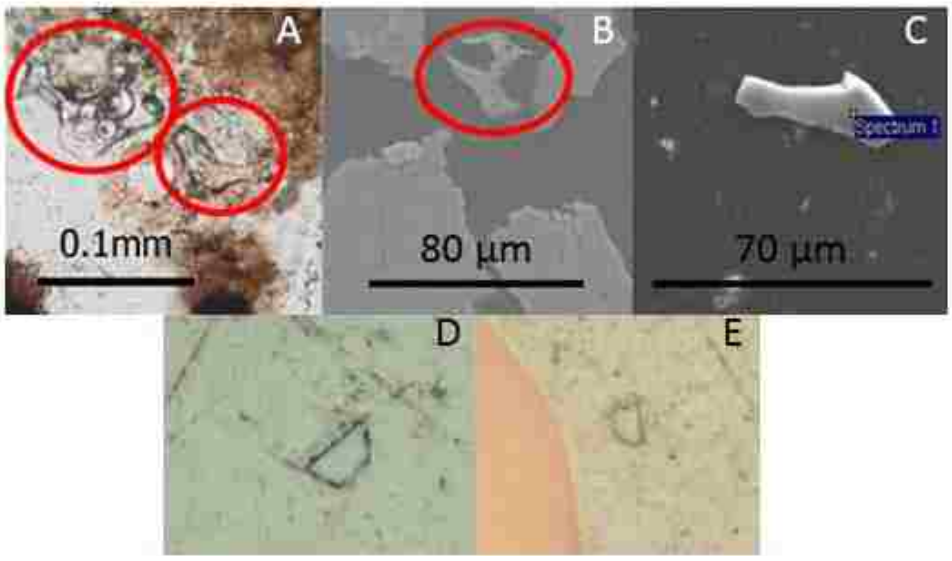

Figure 8: A. Image from petrographic microscope showing two possible shards from the initial discovery made by Panagiotis Karkanas. **B.** Backscatter electron (BSE) image of GS335. **C.** BSE image of 97-shard-A using the SEM. **D.** Photomicrograph of shard 125 in reflected light. **E.** Photomicrograph of shard 49 in reflected light.

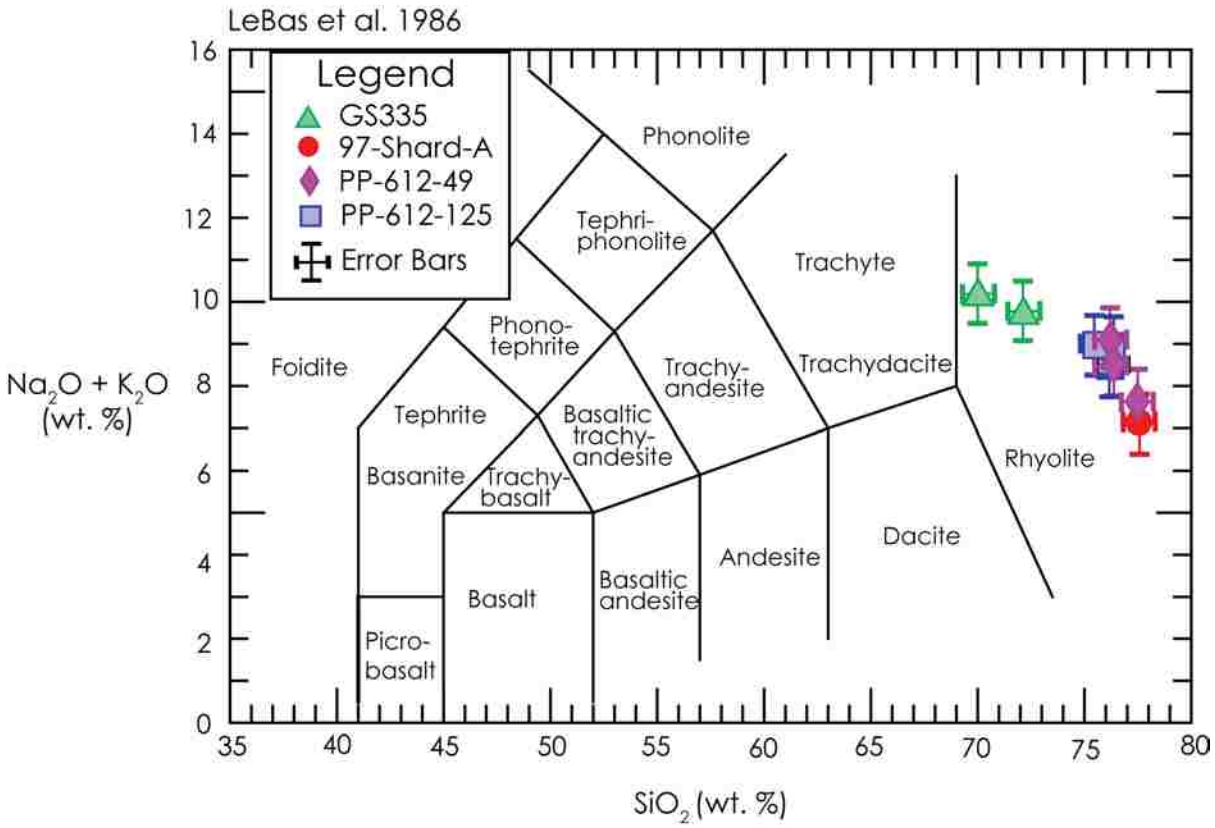

Figure 9: Total alkalis versus SiO_2 diagram of LeBas et al. (1986) showing the variation in the Pinnacle Point shard chemistry. One sigma error bars for $Na_2O + K_2O$ and SiO_2 are denoted based on ATHO-G standard analyses (Table 2). Data are normalized to 100 wt. %.

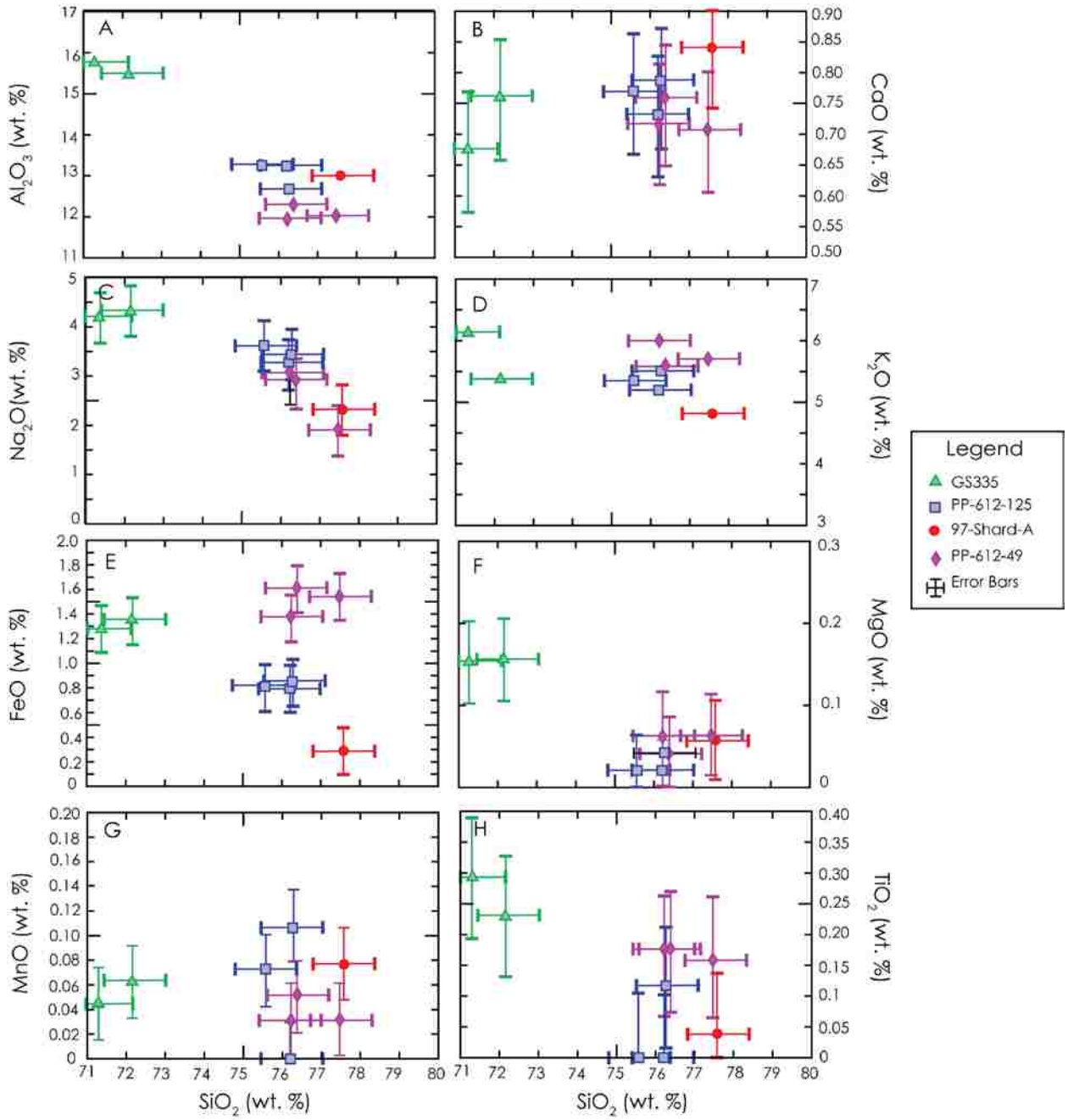

Figure 10: Harker diagrams showing the distribution of major elements for the Pinnacle Point shards (Table 3). One sigma error bars are based on ATHO-G standard analyses (Table 2).

CHAPTER 6: INTERPRETATIONS

The shards in the long section at PP5-6 are spread throughout the SADBS and ALBS stratigraphic aggregates, but peaks and gaps in the distribution may not be significant because of the overall low abundance of shards. The difference between the maximum and minimum abundance of shards is only three shards. Therefore, the most important observation obtained from the distribution profile (Figure 7) is that the first occurrence of shards is in the Conrad Sands sub-aggregate of the ALBS. The position of the first occurrence is nearly the same in both sampling transects and defines an isochron with an OSL age of 73.7±1.9 ka (Smith et al., in prep.).

Possible Sources for Pinnacle Point Shards

It is necessary to look at both nearby and distant sources when matching cryptotephra to a source because tephra can travel long distances and the closest nearby match may not be the correct one (Jensen et al., 2014). Criteria used to search for the source of the Pinnacle Point shards were location, age, and composition.

All possible sources considered for this study are located in the southern hemisphere or equatorial belt. Volcanoes closest to the site would be in central and eastern Africa as well as Antarctica, but tephra from eruptions in Indonesia (Lane et al., 2013) and South America (e.g., the 2011 Puyehue-Cordon Caulle eruption (Klüser et al., 2013)) have reached the African continent.

Although the age of the first occurrence of cryptotephra at PP5-6 is 73.7 ± 1.9 ka, an extended time window of 50-90 ka was used in the search for a source eruption to account for variables such as reworking, dating uncertainty, and the broad distribution of shards in the sediment section. This time window covers the age range of the Long Section in PP5-6. To take into account the reworking of tephra from African volcanoes into younger deposits, volcanic events as old as 700 ka in Africa that produced tephra were also considered as possible sources. The search focused on silicic explosive eruptions that

had the potential for distributing tephra over large areas. However, silicic effusive activity was also included because lava flows and volcanic domes may either be preceded or accompanied by explosive eruptions.

Compositional data for the possible source eruptions as well as volcano names and locations were obtained using the Volcanic Global Risk and Analysis Project (VOGRIPA), and Smithsonian databases of known volcanic eruptions, as well as data from Elmira Wan at the U.S. Geological Survey tephrochronology laboratory and information from the US Geological Survey for Volcanoes of the World database (Mastin et al., 2009). Unfortunately, many databases primarily list Holocene eruptions and rarely extend into Pleistocene eruptions. Therefore, information was also gathered from the published literature.

Africa

The African volcanoes in the Southern Hemisphere and equatorial belt that have had explosive felsic eruptions are located in central and eastern Africa and are part of the East Africa Rift System (EARS; Fontijn et al., 2010; Fontijn et al., 2013). Tephra from the rift volcanoes have been documented in marine deposits up to 2700 km from the source volcanoes (Sarna-Wojcicki et al., 1985, Brown et al., 1992, deMenocal and Brown, 1999 and Peate et al., 2003; Feakins et al., 2007). Therefore, the explosive eruptions that occur in the rift system have the potential of depositing tephra far from the source. The areas in the rift system used for comparison to the Pinnacle Point shards are the Rungwe Volcanic Province (RVP) and the Turkana Basin (Figure 11).

Most of the volcanoes in the EARS are alkaline; the silicic compositions being trachytes and phonolites as well as some rhyolite (McDougall, 1985). The RVP in Tanzania is situated at the intersection of the Malawi Rift, Rukwa/Tanganyika Rift, and Usangu Basin (Fontijn et al., 2010). Ngozi and Rungwe are the two large volcanoes in the RVP that have had documented explosive eruptions

(Fontijn et al., 2010). A third volcano in the RVP, Kyejo, is not considered a possible source because its products are mainly effusive and lack significant tephra (Harkin, 1960; Fontijn et al., 2010; Fontijn et al., 2013). Eruptions from the RVP volcanoes range from basalt and phonolite, to trachyte (Fontijn et al., 2010, Fontijn et al., 2013) and therefore do not match the composition of the PP shards (Figure 12). Although these eruptions are mid-Pleistocene to Holocene in age (0.6 Ma to present), there were no explosive events within the 50 to 90 ka time window.

The Turkana Basin in Kenya and Ethiopia is the only area of the African rift with documented dacite and rhyolite eruptions younger than several million years (McDougall, 1985; McDougall and Brown, 2009). However, these deposits are higher in iron and lower in calcium than the Pinnacle Point shards (Figure 12). The tephra deposits in the Turkana Basin are older than the mid-Pleistocene eruptions in the RVP and range in age from 4.1 to 0.7 Ma (McDougall, 1985).

In summary, the compositions of tephra at the sites in Africa within the time period of interest are mainly alkaline phonolites and trachytes with minor rhyolite. This chemistry does not match the chemistry of the Pinnacle Point shards.

Antarctica

Another possible source of the Pinnacle Point shards is Antarctica. All of the data presented here were obtained from Antarctic ice core records (Siple A, Vostok, Dome C, Dome Fuji, Byrd Station, and Dome C) (Figure 13; Kyle et al., 1981; Narcisi et al., 2005; Basile et al., 2001; Dunbar and Kurbatov, 2011). These ice cores contain a record of Antarctic volcanism as well as distant eruptions from South America and the islands surrounding Antarctica.

There was no high silica rhyolitic volcanism in Antarctica between 50-90 ka recorded in the Siple A, Byrd Station, Dome C, Dome Fuji, or Vostok ice cores (Kyle et al., 1981; Basile et al., 2001; Narcisi et al., 2005; Dunbar and Kurbatov, 2011). Most eruptions represented in the ice cores from Siple A, Dome

C, and Byrd Station are trachytes or trachydacites (Kyle et al., 1981; Dunbar and Kurbatov, 2011). However, other compositions such as trachybasalt, trachyandesite, dacite, and phonolite are documented (Dunbar and Kurbatov, 2011). Dunbar and Kurbatov (2011) also reported a rhyolite with 74.03 wt. % SiO_2; however this rhyolite is less than 40,000 years old. Also, there is tephra in the Siple A core with an age of 70.84 ka. Although similar in age to PP5-6 cryptotephra, this tephra has 62.9 wt. % SiO_2 and is too high in FeO and Na_2O to match the Pinnacle Point shards (Dunbar and Kurbatov, 2011). Other eruptions are too high in Na_2O and FeO and lower in SiO_2 (Figure 14) to match the Pinnacle Point shards. Overall, the composition of tephra from recorded Antarctic eruptions does not match the Pinnacle Point shards.

South America

The Andes are more than 7500 km from Pinnacle Point and are farther from Pinnacle Point than any possible sources in central and east Africa and Antarctica. Most Andean eruptions are intermediate in composition, but there have been rhyolitic eruptions from volcanoes such as Mt. Burney, Reclus, and Aguilera in the Austral Volcano Zone, (AVZ; Stern, 2007). Eruptions from volcanoes in the Southern Volcanic Zone (SVZ) are primarily basaltic to andesitic (Lara et al., 2006). The SVZ has over 60 Quaternary volcanoes as well as three silicic caldera systems (Stern, 2004; Lara et al., 2006). One volcanic system of interest in the southern Andes is the Puyehue-Cordon Caulle Volcanic Complex (PCCVC). The PCCVC has erupted basaltic and silicic lavas, domes, and has produced abundant tephra (Lara et al., 2006). Although many major elements are similar to the PP shards, the Andean rhyolites are lower in K_2O (Figure 15). After detailed comparisons between South American eruptions and PP5-6 shards, it is concluded that volcanism in the Andes did not produce tephra that is a match for the Pinnacle Point shards (Figure 11; Figure 15). However, because we know so little about late Pleistocene volcanism in South America, a source in the Andes cannot be completely ruled out.

Indonesia

The Indonesian Archipelago is thousands of kilometers away from Pinnacle Point in South Africa. However, at least one eruption from Indonesia resulted in tephra deposited on the African continent (Chorn, 2012; Lane et al., 2013). Most rhyolitic eruptions originating in the Indonesian Archipelago occur on the island of Sumatra and the Sunda Strait (Ninkovich, 1979). On Sumatra there are two eruptions that occurred within the time period of interest: the YTT eruption at 74 ka and the 53 ka eruption at Maninjau caldera. There were likely many more eruptions (e.g., Salisbury et al., 2012), but most volcanological research in Sumatra focuses on the largest, the YTT eruption (Alloway et al., 2004). Although Maninjau tephra is nearly identical in major element chemistry to YTT, its eruption was smaller than YYT and produced only 220-250 km^3 of tephra (Purbo-Hadiwidjoyo et al., 1979; Alloway et al., 2004), compared to 2800 km^3 for Toba (Chesner, 2012). The eruption of Maninjau was mainly effusive and lacked a Plinian column (Alloway et al., 2004). Therefore, the only documented Indonesian source for the PP shards is the YTT eruption from the Toba caldera. More background information on the YTT eruption is reported in Appendix D.

Proximal deposits of YTT (such as inside the caldera) show a range of compositions from rhyodacite to high silica rhyolite (Chesner 2012). Distal deposits, however, record only the more silicic end member (Smith et al., 2011; Lane et al., 2013). Most distal Toba analyses have 77-78 wt. % SiO_2 and 12 and 14 wt. % Al_2O_3 (Figure 16A). There is some variability in the chemistry of YTT with one sample having greater than 14 wt. % Al_2O_3. The Pinnacle Point shards, except for GS335, fall within the Toba field for all elements except for FeO and SiO_2. The Pinnacle Point shards are slightly lower in SiO_2 and shard 49 is slightly higher in FeO than the YTT (Figure 16C). There are several possible reasons for the variation between the Pinnacle Point shard chemistry and distal Toba. One of the factors that must be considered is a difference in analytical procedures between different samples. To exclude this possibility, distal Toba tephra from Bukit Sap, Malaysia, provided by Dr. Michael Storey at Roskilde

University in Denmark, was analyzed at UNLV under the same conditions as the Pinnacle Point shards (Table C5). YTT from Malaysia analyzed at UNLV plots in the YTT field for all major and minor elements (Figure 16, black dots). This analytical test indicates that the difference between the chemistry of the Pinnacle Point shards and YTT is due to compositional differences and is not a laboratory issue.

The eruption of YTT not only falls within the 50-90 ka time window, it has chemistry nearly identical to two of the Pinnacle Point shards (Figure 16). Furthermore, the 74 ka age of the eruption agrees with the 73.7 ka OSL age determined for the first appearance of the glass shards in the ALBS. The conclusion is that it is highly plausible that the 74 ka Toba eruption is the source of two of the Pinnacle Point shards.

Shards 97-Shard-A and GS335

There are two shards for which the YTT is not the best match. These are 97-shard-A and GS335. 97-shard-A is considered an outlier because its chemistry cannot be accurately determined from a 52 wt. % total. With normalization, it appears to match the YTT for all major elements except for Na_2O and FeO, and it is probable that if a better analysis were obtained, that 97-shard-A would definitively match the chemistry of the YTT. The 52 wt. % total of 97-shard-A was due to a lack of surface polish on the slide. Unfortunately, this shard was lost during subsequent polishing so no subsequent analyses could be obtained. It is included in Table 3 and the figures as a comparison only. Hence why it is not discussed in the results section.

One possible way to explain the chemistry of GS335 is that the shard suffered beam damage during initial SEM-EDS analysis. The other possibility is that it represents heterogeneity in the cryptotephra deposit and is from a different source. Shard GS335 was analyzed more than 10 times by both SEM and EPMA. The two larger portions of the shard where there is enough material for the beam to hit are separated by a very thin septum. Beam size must be small enough so that epoxy is not

analyzed but large enough to minimize element migration. Due to the small size of the shard, multiple hits occurred in almost the same locations. Re-polishing was conducted twice to expose a new surface to minimize the possibility of altered chemistry due to beam damage. Beam damage from multiple analyses before re-polishing could account for differences in Na_2O and K_2O as well as SiO_2 and Al_2O_3 but should not affect all of the elements (Pearce et al., 2014). Due to the range of SiO_2, Al_2O_3, Na_2O, and K_2O (Table C3, Table C4), beam damage or element migration certainly had an effect during analysis. This leads to the conclusion that beam damage and element migration can become a significant issue when analyzing a shard multiple times. However, even the first analyses of GS335 had lower SiO2 values than the other Pinnacle Point shards which leads to the possibility that GS335 is from a different source that is, at the moment, unknown. A table showing the full set of analyses for GS335 is included in Appendix C.

A Discussion of Pitfalls of Shard Identification and Source Correlation

When first searching for volcanic grains, the objective was to identify classic shard shapes with cuspate margins and vesicles. Shards that matched this description were 97-shard-A and GS335 (Figure 7B and 7C). Shards 125 and 49 typically had nondescript shapes (Figure 8D and 8E). SEM scans to locate the shards first discovered by Karkanas (Figure 7A) were inconclusive. Therefore, there are no chemical analyses for these shards, and it is possible that these shards are opaline material (Appendix C). The presence of abundant opaline material with similar morphology to tephra was a surprising, and pervasive, find. More information on the opaline material can be found in Appendices C and D. Additionally, Visser (2012) in a Master of Science thesis from the University of Utrecht in the Netherlands discusses the visual similarities between tephra and biogenic (opaline) silica.

Many of the grains initially classified as shards with cuspate margins and irregular shapes after electron probe analysis were identified as opaline material (Table C7). The first shard profile was

presented at the Paleoanthropology meeting in 2014 (Smith et al., 2014), but had to be modified when it was discovered that many of the grains identified in the reference slides as shards were actually opaline material (Smith et al., in prep). Once this observation was made, attention was directed at all isotropic grains, regardless of shape. This method proved to be very time-intensive, but the last two analyzed shards were identified using this method.

One of the main challenges of this study was trying to obtain enough shards and data to do robust statistical analyses for geochemically fingerprinting the cryptotephra. Another potential challenge was matching our data and analytical procedure with those used in labs that specialize in analyzing tephra. An example is the Lake Malawi study done by Chorn (2012). In his study, initial analyses were completed by EPMA at the University of Minnesota (UM). Subsequent analyses of the same samples were completed at Oxford University and did not agree with those from UM. Chorn (2012) decided to use the data from the more well-known Oxford lab and discarded the UM analyses. In some studies (e.g., Chorn, 2012), the differences between probe lab analyses are significant and one set of data is discarded for not matching the data coming from the more respected tephra lab. This potential challenge was mitigated for this study by analyzing known YTT tephra from Malaysia and comparing it to published YTT analyses (Figure 16).

Geochemical fingerprinting is a crucial tool in tephrochronology. However, there are several limitations to accurately matching a distal tephra deposit to its source. An important point about matching cryptotephra to a source is that there must be adequate data for the source eruption. Many past eruptions, especially in remote areas, have not been documented or do not have glass geochemistry analyses. This, and if the eruption has not been well dated, leads to a bias in tephra fingerprinting because the databases for matching tephra will have mostly well-known eruptions. This leads to some tephra layers remaining 'unknown' and, until recently, unpublished or matched to the 'best-fit' eruption. Another limitation is alteration/hydration of the glass shards. This limitation is

discussed in Gatti et al., 2014. Many eruptions have similar chemistry for major elements (e.g., Alloway et al., 2004) and distinguishing between them can sometimes be difficult when only using major elements (but most cryptotephra studies still do fingerprinting based on major elements). As tephra frameworks grow, this bias will slowly diminish. In this study, only major elements were used because the size and abundance of shards at Pinnacle Point made finding shards for trace element analysis very difficult.

Figures

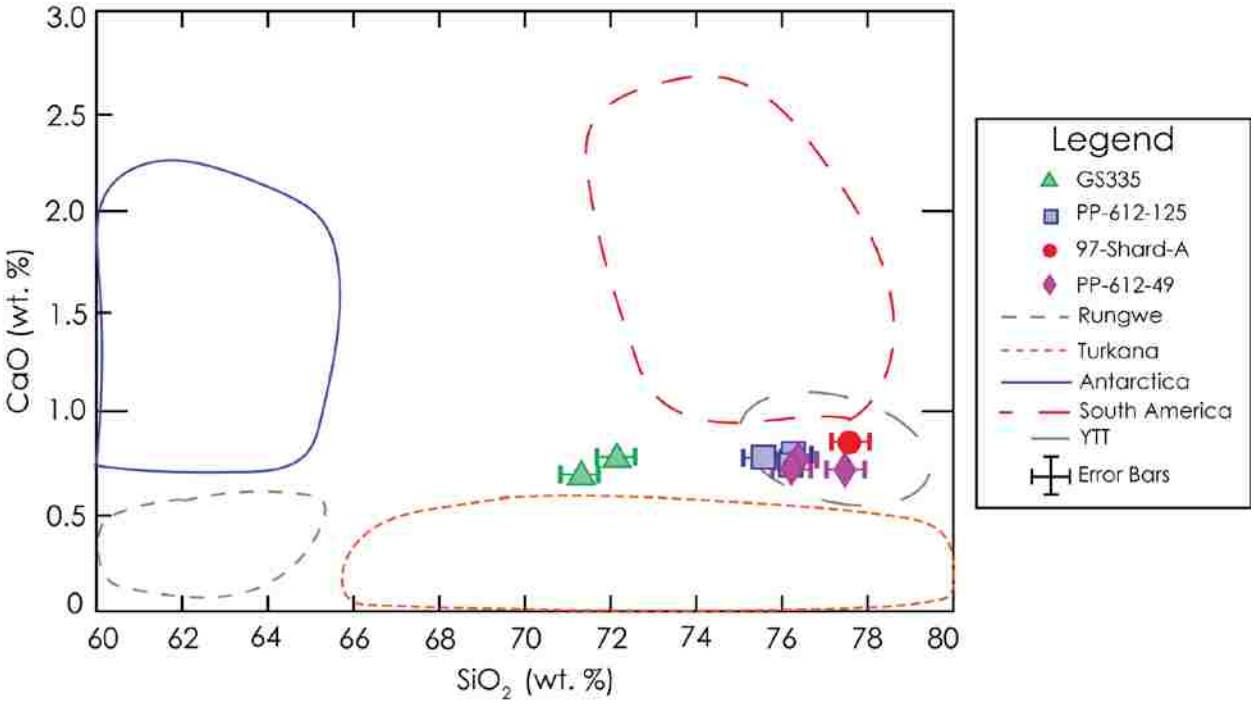

Figure 11: CaO vs. SiO_2 plot comparing the chemistry of Pinnacle Point ELA cryptotephra chemistry to the chemistry of tephra from eastern Africa (Turkana Basin and Rungwe Volcanic Province), Antarctica, South America, and distal Youngest Toba Tuff. NOTE: Some chemistry such as in the Rungwe Volcanic Province in Africa (Fontijn et al., 2010) is whole rock data and not glass chemistry. One sigma error bars were calculated based on ATHO-G standard analyses (Table 2). Error for CaO was smaller than the size of the symbols.

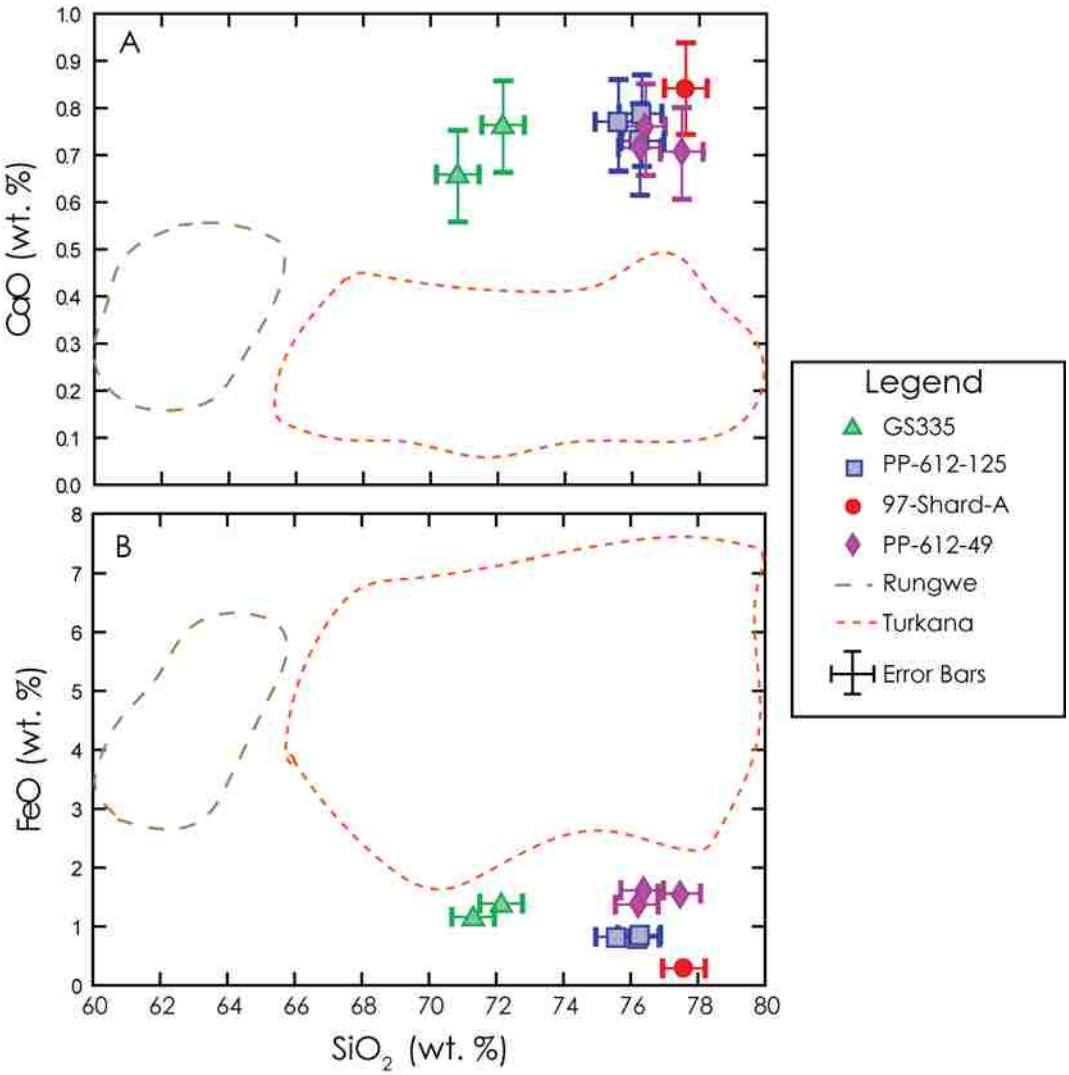

Figure 12: XY plots demonstrating the differences in chemical composition of African volcanism and the PP shards. One sigma error bars were calculated based on ATHO-G standard analyses (Table 2). Error for FeO was smaller than the size of the symbols.

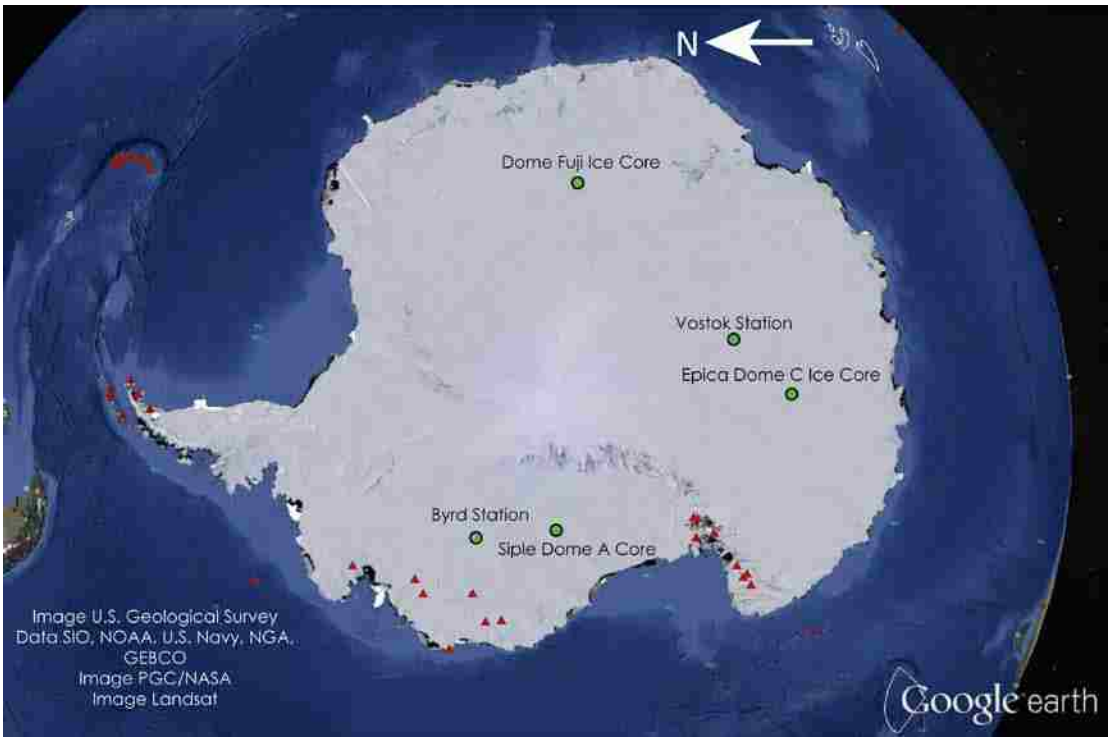

Figure 13: Satellite image of Antarctica. Locations of the Antarctic ice cores used for comparison in this study are represented by green circles, while volcanoes are represented by red triangles.

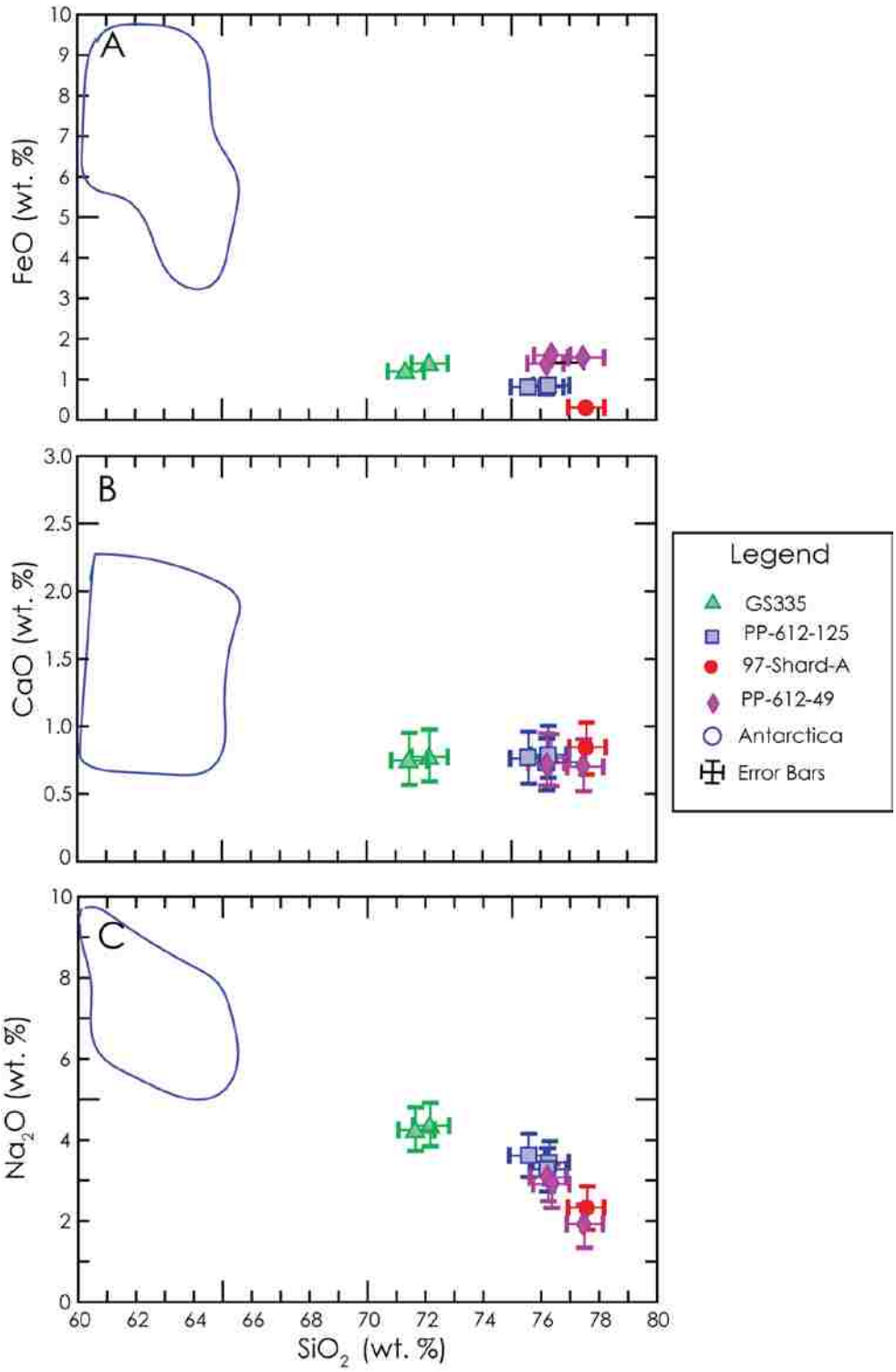

Figure 14: XY plots showing the differences in major elements between Antarctic tephra found in ice cores and the PP shards. Error bars were calculated based on ATHO-G standard analyses for one standard deviation (Table 2).

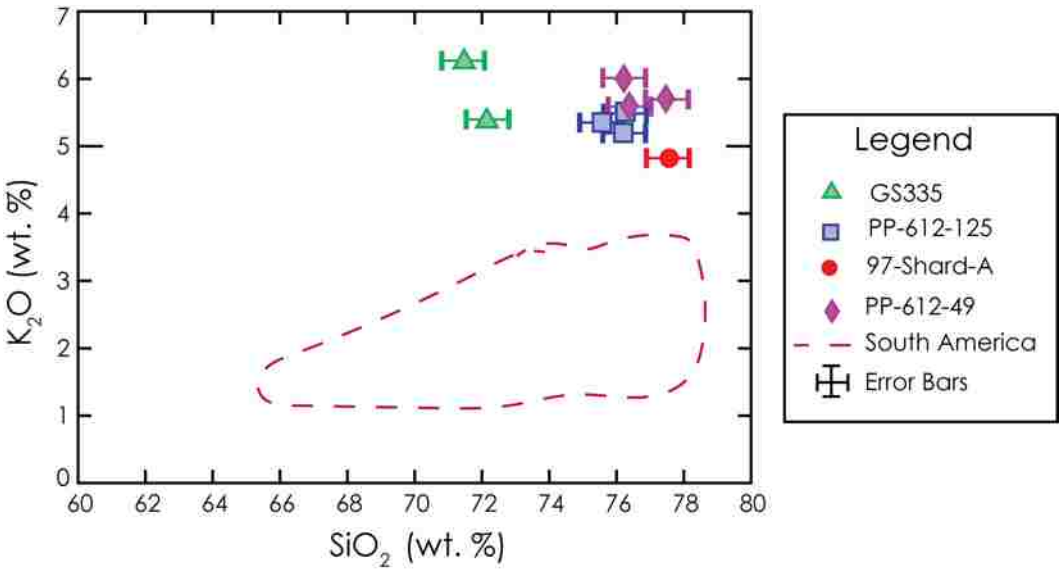

Figure 15: XY plot showing the difference in K_2O between Andean volcanism and the PP shards. Error bars were calculated based on ATHO-G standard analyses for one standard deviation (Table 2).

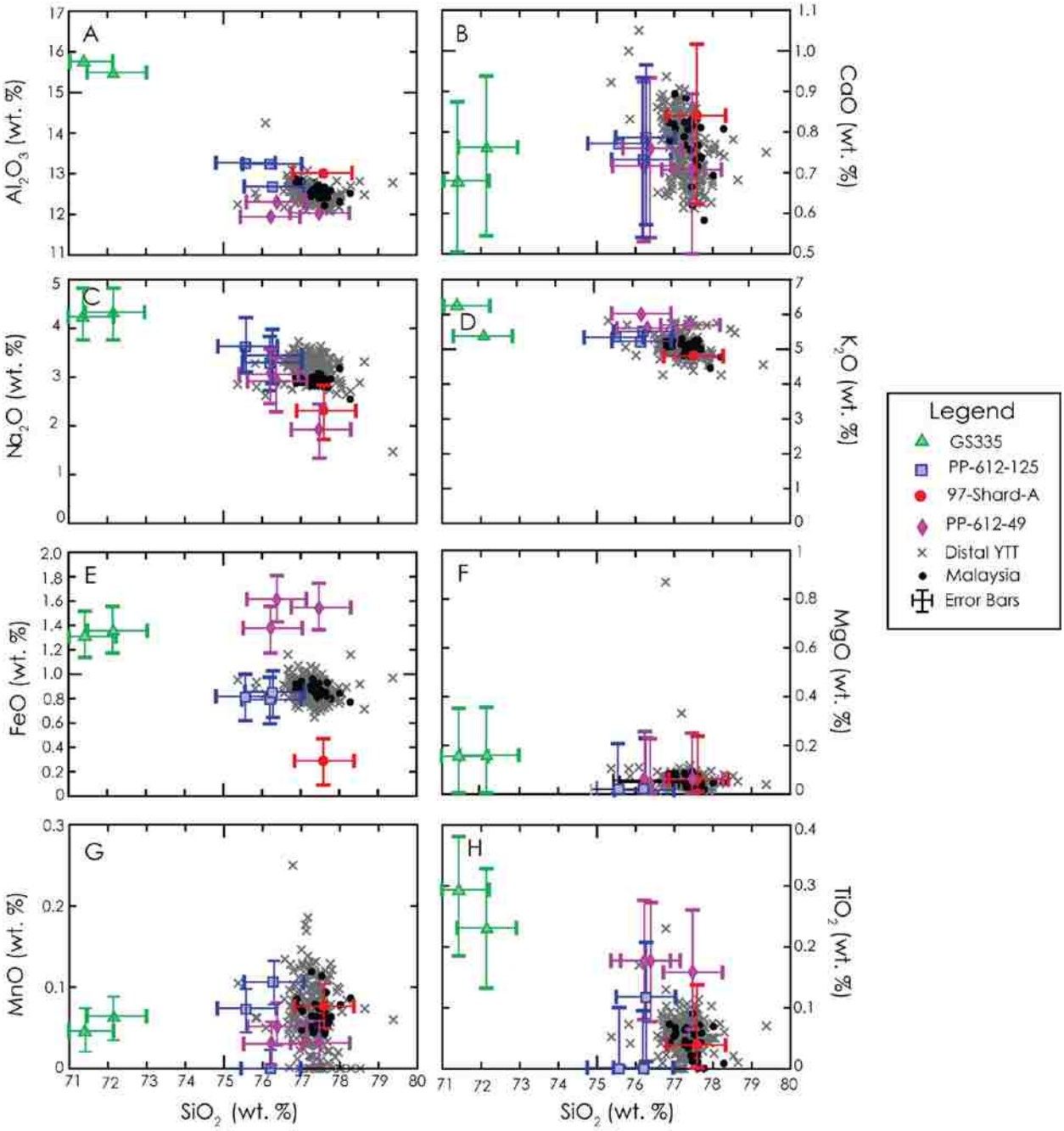

Figure 16: Harker diagrams comparing the multitude of published distal YTT analyses with the chemistry of the Pinnacle Point shards. NOTE: The Malaysia data contains published data (only two analyses) and analyses conducted at UNLV from Bukit Sap. Published YTT data are from Ninkovich et al. (1978); Rose and Chesner (1987); Dehn et al. (1991); Shane et al. (1995); Pattan et al. (1999); Song et al. (2000); Buhring et al. (2000); Gasparotto et al. (2000); Liang et al. (2001); Schulz et al. (2002); Lui et al. (2006); Smith et al. (2011); Gatti et al. (2013); and Lane et al. (2013). Error bars were calculated based on ATHO-G standard analyses for one standard deviation (Table 2).

CHAPTER 7: CONCLUSIONS

This study is part of a larger ELA cryptotephra project at PP5-6 that includes the surrounding Stratigraphic Aggregates within PP5-6 and other sites in South Africa. This project aims to find more cryptotephra in South African archaeological sites to create a regional framework for ELA cryptotephra and create a well-constrained age tie point for artifacts found in the area. The major conclusions of this study are:

1. Shards of volcanic origin have been identified in rock shelter PP5-6 near Mossel Bay, South Africa.
2. Based on comparisons to available geochemical data in international volcano databases, the best fit for the source of the shards is the 74 ka eruption of the YTT from the Toba caldera in Indonesia.
3. The shards are found at the same stratigraphic position in several sampling profiles. The OSL date of the stratigraphic horizon is 73.7 ka. There is excellent correlation of the OSL date and the age of the horizon determined by the age of the YTT.
4. The first occurrence of the YTT defines an isochron that helps to tie the PP5-6 sediment section to other sections in India and Southeast Asia that contain YTT.

An important lesson learned from this study is that while extracting ELA cryptotephra can be done, it is time and labor intensive. It is still early in the evolution of ELA cryptotephra research and many techniques used to categorize tephra deposits and cryptotephra layers (such as statistical calculations: similarity coefficients, and principle component analysis) cannot be used when dealing with ELA cryptotephra. Separation techniques for ELA cryptotephra have to be more specialized than those used for cryptotephra layers with hundreds or thousands of shards and have a higher chance of lab contamination.

In conclusion, more work is needed to create tephra frameworks in Africa for the late Pleistocene and in areas away from the rift zone, especially in archaeological deposits. This is necessary in order to determine the extent of African tephra deposits as well as document the presence of tephra from other regions (i.e., Aegean tephra in North Africa; Barton et al., 2015).

APPENDIX A: EXTENDED METHODS

Lab Manual and Methods Experiments

The lab separation procedures used at UNLV includes 3 phases of separations: acid digestion, sieving (size separation), and heavy liquid separation. While processing samples, experiments/modifications were performed to determine what practices were most time efficient and practical.

- Label 50 mL conical tubes with sample numbers.
    - Experiment 1 (Pre-sieving): Some samples contained artifacts and other large material. For these samples, sieving before weighing removed these particles. However, this should be done carefully to not introduce contaminants into the sample. This step reduced the amount of large particles present in Phase 2.
- Place approximately 1 gram of sample into the tubes. Record the exact weight.

Phase 1: Acid Digestion

- Place the tubes in a rack and put it in a fume hood.
- Use 10% HCl to dissolve carbonates.
    - Unless the sample is full of carbonate material, 15 ml should be enough.
- Stir/shake the tube to make sure the acid reaches all of the sediment.
- When the acid stops fizzing (or mostly stops), put the caps back on the tubes.
    - Make sure you do not tighten the caps all the way, leave them loosened.
- Leave the tubes in the fume hood with loosened caps overnight.
    - This is to give time for the acid to continue dissolving carbonates even if it looks like it finishes quickly.
    - Leave a note on the fume hood warning people that the caps on the tubes are loose and should not be touched.

Phase 2: Wet Sieving

- Set up wet sieving station. This includes two plastic sieve frames with removable mesh. One sieve will have nylon 80-micrometer mesh while the other will use nylon or polyester 20-micrometer mesh.
    - Experiment 2 (Nylon vs. Polyester Mesh): Nylon mesh is better for abrasion while polyester is more resistant to acids. For the Normesh sieves, nylon is ideal. This is because the Normesh sieves provide a very tight fit. When separating the sieve frame, the mesh may gain small tears. This was most prevalent in the polyester mesh. However, the nylon mesh absorbs a small amount of water, which makes it much harder to separate the sieve frame. These frames are already very difficult to separate.
    - Experiment 3 (Normesh vs. Bel-Art Sieves): This experiment is currently being conducted. The Normesh sieves provide twice the sieve area while the Bel-Art sieves come in a pack of 4 and have a smaller diameter. The Bel-Art sieves are also half as expensive as the Normesh sieves which have to be shipped from the UK. So far, the Bel-Art sieves are easier to separate and use than the Normesh sieves. Plastic sieve frames were also obtained from Global Gilson. These frames were 8 inches in diameter and were much shallower than both the Normesh and Bel-Art sieves. The sediment tends to jump while using the spatula so greater depth is ideal.
- Take the 50 mL tubes used for acid digestion out of the fume hood after tightening the caps.
- Pour the material from the first tube into the sieve with the 80-micrometer mesh. Use a squirt bottle with DI water to make sure all of the material from the tube comes out.

    - Also rinse off the cap (material sometimes gets stuck there if you shake the tube during acid digestion).
    - RO water can be used for this stage but DI water is necessary for Phase 3.
- Use a “goo spreader” (mini spatula) to move the material around in the sieve.
    - This action plus using the water squirt bottle will push the finer material through the mesh and into the beaker below. Continue to do this until the water coming out of the funnel is clear.
    - For organic-rich samples, this process will take longer. Spending more time in Phase 2 for these samples will save time in Phase 3.
- Then tilt the sieve up on one side and push all of the material to one end.
- Use the spatula and squirt bottle the same as before and check if the water coming out of the funnel is clear. If it is still clear, move to the next sieve.
- Depending on how much water used during the first part of sieving, the beaker may become full before finishing. In this case, pour some of the water from the first beaker into the second sieve holding the 20-micrometer mesh.
    - This sieve will take longer for water to pass through so it is okay to periodically dump water from the first beaker into the second sieve several times before finishing with the first sieving.
- Once finished with the 80-micrometer sieve, pour water from that beaker into the second sieve.
    - Use the squirt bottle to make sure all of the material from the beaker goes into the sieve.
- Take the material left in the first sieve and pour it back into the 50 mL tube it was in before.
    - Do this using a small funnel.
    - This will now be the tube containing “too coarse” material for this sample.

    - Keep this material. If large shards are found, go through this material to see if there are any shards larger than 80 micrometers.
        - Experiment 4 (Large Opal): Many of the Pinnacle Point samples contained opaline material. This material was also present in the larger size fraction. No shards have been found in the larger size fraction.
- Then separate the sieve frame without messing up the mesh. There will still be a little material left on it. Use the squirt bottle to rinse this excess material into the tube.
    - Be careful not to overfill the tube!!!! This will be very important when using the smaller 15 mL tubes.
    - Also rinse the outer rim of the sieve, especially where the sieve frame meets the mesh. This area sometimes catches sediment.
- Repeat all of the previous sieve steps.
- Put the material left on the 20-micrometer mesh into a 15 mL-rounded bottom tube.
    - This is the material that will go through heavy liquid separation.
- Discard the <20-micrometer material in the beaker.
    - Material from this beaker can be dumped.
    - Note: Check if the sinks have a sediment catch.

Phase 3: LMT Separation

The next part of the extraction process involves heavy liquid separation using LMT (Lithium Metatungstate), which has to be mixed with water to achieve the right density for separation. The two densities used for the separation technique are 1.95 g/cm3 and 2.55 g/cm3.

Pre-Cleaning Phase

- Top off all of the new 15 mL tubes of sediment with DI water.
    - This is to keep the centrifuge balanced.

- Load into centrifuge and centrifuge for 5 minutes at 2500 rpm.
- Repeat the previous 2 steps twice.

Main Phase

- Use a pipetter to put 4 ml of LMT (1.95 g/cm3) into each of the 15 ml tubes.
- Centrifuge for 15 minutes at 2500 rpm.
- Pour the float into a 15 ml conical tube labeled <1.95.
- Repeat the 3 previous steps once.
    - These repetitions are to catch any lingering material that may have been missed in the first round. This is very important is samples that are rich in organic material.
- Use a pipetter to put 2.55 g/cm^3 LMT into the original 15 mL tubes and repeat all of the previous steps of the main phase.
    - The float of this round is poured into new 15 mL conical tubes labeled 1.95-2.55.
    - This float is the density fraction used to find the glass shards.
        - <u>Experiment 5 (Different Densities):</u> Current experiments are being conducted changing the densities of the LMT. These changes are to separate the shards from the opaline material that is so prevalent in the samples. This was not done earlier in the project because others have noted little difference (Visser, 2012). However, this is being revisited due to the extent of the opaline material problem. The new/added density is around 2.2 or 2.3 g/cm^3.

Final Cleaning Phase

The tubes must now be cleaned and the LMT recycled. This is a two-step process. The tubes to be cleaned are the original 15 mL round tubes and both sets of conical tubes. The nature of these tubes and careful pouring will keep any sediment from being lost during this process.

- First top off all tubes with DI water.

- Then centrifuge all tubes for 5 minutes at 2500 rpm and pour liquid out into a 1000 mL beaker for LMT recycling. Repeat this process twice.
- The material left in the 1.95-2.55 tube is what will be used to make reference slides and for shard picking. The rest will be kept in storage.
    - Experiment 6 (final sieving vs. increased cleaning reps): The Oxford lab uses a final sieving round before mounting the sediment on slides. This is to get rid of any remnant LMT after cleaning. Increased cleaning rounds should also get rid of this LMT. However, both of these made little difference in this study.
    - Experiment 7 (15mL vs. 50 mL cleaning tubes): This is a current experiment. The 50 mL tubes will be used in the final repetition of cleaning. This is to try to extract the last bit of remnant LMT from the samples. This LMT is too minute to be recycled/reclaimed but it crystallizes on the slides and may cause pealing during grinding.

Making Slides

Microscope slides are made as a reference for shard counting. These slides are used to determine (identify) how many shards are present in the samples and to make a shard frequency diagram.

- To make the reference slides, find Canada balsam (or equivalent epoxy for mounting), a hot plate, microscope slides, a bamboo skewer, and disposable pipettes. (for epoxy mounting you only need the hot plate, slides, and pipettes)
- Label the microscope slides before proceeding. I draw boxes on the underside with sharpie.
- Place the slides onto the hot plate.
- Turn the hot plate on but make sure the temperature is below boiling.
    - You do not want the water to bubble. Bubbling water may cause sediment to jump off the slide.

- Use the pipette to mix up the sediment in the tubes by sucking the water into the pipette and pushing it back out.
- Use the pipettes to carefully drop water with the sediment (from the tubes) onto the middle of the slides.
    - Do not put more than three drops on the slides at any given time.
    - The water will run and has to be watched carefully. The heat from the hot plate will evaporate the water and leave just the sediment behind on the slide.
- For Epoxy Setting: Take the slides off the hot plate and use a beaker to cover them until cool.
- Mix the epoxy one batch at a one for at least 3 minutes (slowly). Use the pipettes to drop epoxy onto the slides.
- Leave slides to cure overnight.
    - Experiment 8 (Epothin vs. Epothin 2 vs. Specifix): Three types of epoxy were used at different points in this study. Specifix was used in Oxford to create the shard picking rounds. It is clear and uses heat to cure within a few hours. It can be mixed quickly and when cured, is relatively bubble-free. Epothin epoxy was used for the majority of this study. It was an older bottle so these observations may not be useful for new Epothin epoxy. It cures without using heat within 24 hours and has a yellow tinge. If mixed slowly, it is relatively bubble-free. It turns slightly more yellow on the hotplate. Epothin 2 is the most recent epoxy used in this study. It is less viscous/easier to spread than the Epothin epoxy and is clearer in color. It also has a perfume type scent that permeates the area. NOTE: Both Epothin and Epothin 2 have a peak temperature of 86 degrees Fahrenheit.
    - Experiment 9 (epoxy vs. Canada Balsam): Epoxy is used in this study. Epoxy is a more permanent setting than Canada Balsam. With epoxy, the slides can be

scanned for shards and then polished for analysis. Canada Balsam slides use a cover slip and cannot be put in the microprobe. The downside of epoxy is that if it cures improperly, the slide is ruined. This happened several times with the Epothin epoxy. Epoxied slides that have been ground for analysis also cannot be revisited for subsequent shard counting/checking.

- Experiment 10 (plain slide vs. epoxy covered): This experiment was conducted to try to lessen pealing of the epoxy when ground very thin. The sediment sits right on the slide and does not rise through the epoxy. Hence, they must be ground very close to the slide if there are shards for analysis. Covering the slides with a layer of epoxy made it somewhat easier to grind the slides for analysis. However, it did not seem to help with pealing of the top layer of epoxy. The pealing is now thought to be because of a minor amount of remnant LMT that crystallized on the slides. Epoxy covered slides were used for the majority of this study.

- For Canada Balsam setting: Once all of the sediment is out of the tubes, take a cover slip and put Canada Balsam on it with a bamboo skewer.
- Then carefully place the cover slip over the area on the slide that contains the sediment.
- Move the slide to the edge of the hot plate so it can cool and then put the slide onto a tray to set.
- Once the slides are done setting, take them to the microscope and count the number of shards in each and document with a few pictures.
- Note the shape of the shards and characteristics.
- Be careful not to confuse shards with phytoliths and opaline material.

- Phytoliths and other opaline material are very prevalent in these samples and sometimes look very similar to the shards (Appendix E; Visser, 2012).

Polishing

- Locate the shard, record coordinates and take a picture. Use reflected light to bring the surface into focus and then see how long it takes for the shard to focus.
- If it is far from the surface, use 240 grit for a while. Then go to 800 to polish it for viewing.
- Once the shard is only a few "turns" away from the surface, switch to 600 or 800 grit.
- Periodically use 1200 to give some polish for viewing.
- Once you can see the "shadow" of grains at the surface, start being careful about scratches and grinding too far.
- Once you can use just fine tuning to focus the surface and the shard, use only 1200 grit or move to polishing pads.

Making LMT

Making LMT is easier than making SPT. LMT from (lmtliquid.com) comes as a liquid in liter bottles. SPT is sold in powder form and must be hydrated before use. This makes LMT preparation quicker but SPT has one advantage. When bringing the heavy liquid to the densities for use, the crystallized SPT can be used to increase the density if the solution becomes too dilute. With LMT, this is also possible if leftover original LMT is available. Otherwise, the solution must be heated to evaporate some of the water and increase the density.

- Experiment 11 (LMT vs. SPT): This experiment is currently underway. Ideally, LMT and SPT should be interchangeable so there should be no difference between using LMT or SPT. This experiment is to assess which heavy liquid is more cost effective and less time consuming to make.

Dilution

The densities used for this thesis were 1.95 and 2.55 g/cm3. Dilution was conducted so that a large amount of LMT of the right densities is made at once instead of diluting before every set of separations. The amount made is based off of the amount of LMT available for dilution and hydrometer length. Batches of 500 mL and 250 mL were primarily used.

- Make 2.55 g/cm^3 LMT first.
- Pour high density LMT into graduated cylinder (or testing cylinder). Fill more than halfway.
- Pour in DI water. The ratio of LMT and DI water depends on the starting density of the LMT.
    - It is important to use DI water here. We were using RO water. This caused a calcium precipitate to form at the bottom of the cylinders.
    - The LMT and DI water will not immediately mix. It must be shaken.
- Place parafilm tightly over the top of the cylinder.
    - This is to provide a seal for those of us with small hands.
- Put hand over the top of the cylinder and slowly tip it upside down and right side up again.
    - Do this multiple times. This is to mix the LMT and DI water.
- Set cylinder down onto tray and take off the parafilm.
- Use a hydrometer to test the density of the solution.
    - It is better to have hydrometers with the optimal densities towards the bottom instead of the top. This way, less LMT needs to be made in order for the hydrometer to be used.
- If the density is too high, add more DI water and previous 4 steps. If the density is too low, add more high density LMT. If none is available, pour LMT solution into a beaker and heat in an oven or on a hotplate.
    - It is easier to fix a density that is too high rather than one that is too low.

- Once the density is around 2.55 g/cm^3, put parafilm over the cylinder.
    - If not using the cylinder to store the LMT solution, pour into another container.
- For making the 1.95 g/cm^3 LMT, either excess 2.55 g/cm^3 LMT can be used or the high density LMT.
- Repeat steps used for making the 2.55 g/cm^3 LMT.
    - Use less LMT and more water for this one than the 2.55 g/cm3 LMT.
- Test density with a hydrometer.
    - A too low density is easier to deal with here. Just use a little bit of the newly made 2.55 g/cm^3 LMT.
- Once the density is around 1.95 g/cm^3, put parafilm over the cylinder for storage.

Recycling LMT

Recycling or reclaiming LMT is very similar to reclaiming SPT. A general schematic and process for it can be found on the manufacturer's website: lmtliquids.com. To reclaim the used LMT, filter paper of three pore sizes were used: about 25 micrometer, 5-8 micrometer, and about 1 micrometer. This process requires filter paper, beakers, ring stands with o-clamps, funnels, and an oven or hotplate. The filtering occurs in 3 steps.

- Place a funnel on a ring stand with o-clamps directly over an empty beaker.
- Fold 25-micrometer filter paper to fit in funnel.
    - Quality grade is best for this type of work (see Whatman's filter paper guide). Ashless, hardened, and quantitative types are not needed because the sediment on the filters will not be analyzed.
    - The filter paper should have a good wet strength and medium to high flow rate.

        - Experiment 12 (flat vs. fluted filter paper): Flat filter paper is typically okay for most applications and is cheaper and easier to find than fluted/pleated versions. However, if not folded carefully or used too much, minute tears can let sediment through the filter where it was folded. Fluted filter paper is already pleated and looks like a generic coffee filter. Because of the pleats, it has increased surface area for the LMT to filter through and sticks less to the sides of the funnel than the flat filter paper.

- Place filter paper into funnel and make sure the funnel is aligned on top of the beaker.
    - Do not have the funnel too high above the beaker. Otherwise, the LMT will splash and potential make a mess.
- Slowly pour the used LMT over the filter paper.
    - If the LMT solution is very dilute, more can be poured in. However, too much (this is more true for the higher density LMT solutions than very dilute ones) at once can cause the filter paper to tear.
        - Experiment 13 (Single filtering vs. stacked filtering): Filtering can be done faster if there are multiple tiers of funnels and filter paper on the same ring stand. This is much faster than single filtering, but the filter papers all have different flow rates. If the finer filter paper has a flow rate much slower than the coarse filter paper, too much of the LMT solution may filter through the coarse paper and overflow the much slower filtering fine paper. This can be avoided by pouring very small amounts of LMT solution at a time or finding filter paper with similar flow rates. Stacked filtering was used for a majority of this study. Single filtering is more time consuming than stacked filtering but does not come with problems of overflowing the filter paper.

- Once initial filtering of the beaker is complete, place a quartz crystal into the beaker.
    - This is to monitor the density of the LMT solution.
- Place the beaker into the oven or onto a hot plate.
    - If using a hot plate, use a combination hot plate and magnetic stirrer. Place a stirring rod into the beaker.
- Evaporating the water from the LMT solution will take multiple hours.
    - Do not let the LMT solution boil and bubble.
    - It is done when the quartz crystal floats.
- After the LMT is at higher density (2.65 g/cm^3), filter using 1 micrometer filter paper.
    - Pour very slowly, this filter has a slow flow rate.
    - Pouring too much too fast will result in minute tears and part of the LMT crystallizing on the filter.
- After filtering using 1-micrometer filter paper, pour the reclaimed LMT into a bottle for storage.

Equipment and Supply List

Table A1: Equipment at the UNLV Cryptotephra Extraction Lab.

Equipment	Quantity	Source
Centrifuge	1	www.amazon.com
Oven	2	UNLV
Manual Micromanipulator	1	www.harvardapparatus.com
Hot Plate/Magnetic Stirrer	2	UNLV
Petrographic Microscope w/ camera	1	UNLV
Weighing Balance	3	UNLV
Ultrasonic Cleaner	3	UNLV

Table A2: General list of supplies used at the UNLV Cryptotephra Extraction Lab.

Supply	Source
LMT	Lmtliquid.com
Graduated Cylinders	UNLV
Density test cylinder	www.fishersci.com
Sieve Frames	www.globalgilson.com (8 inch) www.normesh.co.uk (6 inch) www.fishersci.com (3 inch)
Sieve mesh	www.elkofilter.com
Hydrometers	www.fishersci.com
Pipetter	www.fishersci.com
1000 mL Glass Beakers	www.fishersci.com
1000 mL Plastic Beakers	www.amazon.com
Pipette Tips	www.fishersci.com
15 mL tubes (Celltreat)	www.fishersci.com
50 mL tubes	www.amazon.com
15 mL round bottom tubes	www.amazon.com
Disposable Pippette	www.fishersci.com
Funnels	www.amazon.com
Bottles	us.vwr.com/store
Petrographic slides	us.vwr.com/store
Small beakers	www.fishersci.com
HCl	www.fishersci.com
Nitric Acid	us.vwr.com/store
Filter Paper	www.fishersci.com
Ring Stand and clamps	www.fishersci.com
Small “goo spreaders”	www.amazon.com
Magnetic stirrer	www.amazon.com
10 microliter glass syringe	www.fishersci.com
100 mm silica syringe needle	www.fishersci.com
Nitrile disposable gloves	us.vwr.com/store
Petrographic slide box	us.vwr.com/store
Lab jack	www.amazon.com
Test tube racks	www.fishersci.com
Quartz crystals	www.amazon.com
Single cavity microscope slides	www.amazon.com
Kim wipes	us.vwr.com/store
Epothin	UNLV
Grinding Paper	UNLV
Aluminium Polishing Paste	UNLV
Epoxy molds	UNLV
Bamboo skewers	www.amazon.com

APPENDIX B: EXTENDED FIELD DATA

Table B1: Sample Numbers and Stratigraphic Position

Sample Number	Barcode	Stratigraphic Aggregate	Height from Sub-Agg Base
PP-612-1	357200	Kim	0.129949
PP-612-2	357201	Kim	0.119624
PP-612-3	357202	Kim	0.108541
PP-612-4	357203	Kim	0.088674
PP-612-5	357204	Enrico	0.074978
PP-612-6	357205	Enrico	0.062448
PP-612-7	357206	Enrico	0.047641
PP-612-8	357207	Enrico	0.022176
PP-612-9	357208	Enrico	0.005641
PP-612-10	357209	Gert	0.134587
PP-612-11	357210	Gert	0.125398
PP-612-12	357211	Gert	0.110581
PP-612-13	357212	Gert	0.098862
PP-612-14	357213	Gert	0.089206
PP-612-15	357214	Gert	0.079684
PP-612-16	357215	Gert	0.070991
PP-612-17	357216	Gert	0.062333
PP-612-18	357217	Gert	0.049635
PP-612-19	357218	Gert	0.040214
PP-612-20	357219	Gert	0.031638
PP-612-21	357220	Gert	0.022127
PP-612-22	357221	Gert	0.014087
PP-612-23	357222	Gert	0.002254
PP-612-24	357223	Holly	0.002254
PP-612-25	357224	Holly	0.029813
PP-612-26	357225	Holly	0.00981
PP-612-27	357226	Sydney	0.0841
PP-612-28	357227	Sydney	0.067598
PP-612-29	357228	Sydney	0.049971
PP-612-30	357229	Sydney	0.03851
PP-612-31	357230	Sydney	0.030888
PP-612-32	357231	Sydney	0.016167
PP-612-33	357232	Sydney	0.004649
PP-612-34	357233	Sydney	0.049986
PP-612-35	357234	Sydney	0.036505
PP-612-36	357235	Thandesizwe	0.145093
PP-612-37	357236	Thandesizwe	0.136414
PP-612-38	357237	Thandesizwe	0.129655
PP-612-39	357238	Thandesizwe	0.116878
PP-612-40	357239	Thandesizwe	0.106867
PP-612-41	357240	Thandesizwe	0.090779
PP-612-42	357241	Thandesizwe	0.074755
PP-612-43	357242	Thandesizwe	0.060786
PP-612-44	357243	Thandesizwe	0.045319
PP-612-45	357244	Thandesizwe	0.030014
PP-612-46	357245	Thandesizwe	0.01344
PP-612-47	357246	Erich	0.055463
PP-612-48	357247	Erich	0.043513
PP-612-49	357248	Erich	0.035027
PP-612-50	357249	Erich	0.017951
PP-612-51	357250	Erich	0.008843
PP-612-52	357251	Jocelyn	0.175899

PP-612-53	357252	Jocelyn	0.162964
PP-612-54	357253	Jocelyn	0.153143
PP-612-55	357254	Jocelyn	0.14406
PP-612-56	357255	Jocelyn	0.13876
PP-612-57	357256	Jocelyn	0.113165
PP-612-58	357257	Jocelyn	0.10662
PP-612-59	357258	Jocelyn	0.098574
PP-612-60	357259	Jocelyn	0.081832
PP-612-61	357260	Jocelyn	0.067813
PP-612-62	357261	Jocelyn	0.042078
PP-612-63	357262	Conrad Sands	0.206097
PP-612-64	357263	Conrad Sands	0.185726
PP-612-65	357264	Conrad Sands	0.16831
PP-612-66	357265	Conrad Sands	0.157239
PP-612-67	357266	Conrad Sands	0.150694
PP-612-68	357267	Conrad Sands	0.140758
PP-612-69	357268	Conrad Sands	0.132444
PP-612-70	357269	Conrad Sands	0.124221
PP-612-71	357270	Conrad Sands	0.113073
PP-612-72	357271	Conrad Sands	0.102108
PP-612-73	357272	Conrad Sands	0.092559
PP-612-74	357273	Conrad Sands	0.08532
PP-612-75	357274	Conrad Sands	0.070281
PP-612-76	357275	Conrad Sands	0.057553
PP-612-77	357276	Conrad Sands	0.045573
PP-612-78	357277	Conrad Sands	0.033563
PP-612-79	357278	Conrad Sands	0.01949
PP-612-80	357279	Conrad Sands	-0.000163
PP-612-81	357280	Conrad Cobble and Sand	0.294707
PP-612-82	357281	Conrad Cobble and Sand	0.285002
PP-612-83	357282	Conrad Cobble and Sand	0.274445
PP-612-84	357283	Conrad Cobble and Sand	0.259143
PP-612-85	357284	Conrad Cobble and Sand	0.240269
PP-612-86	357285	Conrad Cobble and Sand	0.225381
PP-612-87	357286	Conrad Cobble and Sand	0.215319
PP-612-88	357287	Gert	0.042707
PP-612-89	357288	Gert	0.032665
PP-612-90	357289	Gert	0.023395
PP-612-91	357290	Gert	0.009773
PP-612-92	357291	Gert	0.000159
PP-612-93	357292	Holly	0.039142
PP-612-94	357293	Holly	0.02602
PP-612-95	357294	Holly	0.014424
PP-612-96	357295	Sydney	0.138305
PP-612-97	357296	Sydney	0.126102
PP-612-98	357297	Sydney	0.110662
PP-612-99	357298	Sydney	0.097456
PP-612-100	357299	Sydney	0.080408
PP-612-101	357300	Sydney	0.05804
PP-612-102	357301	Sydney	0.038023
PP-612-103	357302	Sydney	0.023082
PP-612-104	357303	Thandesizwe	0.143027
PP-612-105	357304	Thandesizwe	0.12558
PP-612-106	357305	Thandesizwe	0.10848
PP-612-107	357306	Thandesizwe	0.087492
PP-612-108	357307	Thandesizwe	0.076481

PP-612-109	357308	Thandesizwe	0.046952
PP-612-110	357309	Erich	0.05927
PP-612-111	357310	Erich	0.009982
PP-612-112	357311	Erich	-0.000221
PP-612-113	357312	Jocelyn	0.148765
PP-612-114	357313	Jocelyn	0.129933
PP-612-115	357314	Jocelyn	0.122135
PP-612-116	357315	Jocelyn	0.104289
PP-612-117	357316	Jocelyn	0.091862
PP-612-118	357317	Jocelyn	0.077526
PP-612-119	357318	Jocelyn	0.05887
PP-612-120	357319	Jocelyn	0.022458
PP-612-121	357320	Jocelyn	0.000333
PP-612-122	357321	Conrad Sands	0.10272
PP-612-123	357322	Conrad Sands	0.080681
PP-612-124	357323	Conrad Sands	0.069952
PP-612-125	357324	Conrad Sands	0.058337
PP-612-126	357325	Conrad Sands	0.046755
PP-612-127	357326	Conrad Sands	0.037102
PP-612-128	357327	Conrad Sands	0.022686
PP-612-129	357328	Conrad Sands	0.012215
PP-612-130	357329	Conrad Sands	0.003609

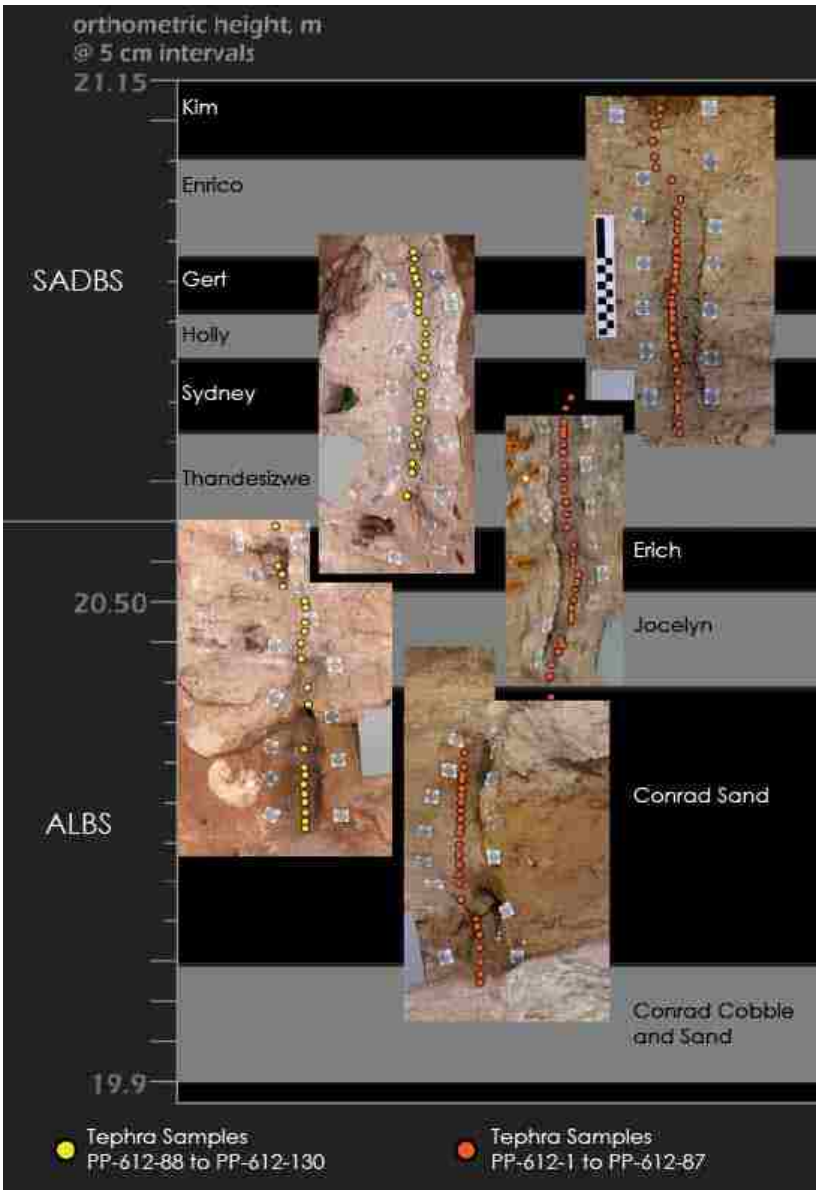

Figure B1: Stratigraphic position of the samples collected in 2012 by Smith and Keenan. Figure modified from Smith et al. (2014).

APPENDIX C: EXTENDED RESULTS

Shard Data

Table C1: Analyses for 97-Shard-A, both EPMA and SEM as well as standard analyses. An analysis on the glass slide was conducted to ensure that 97-shard-A was not a fragment of the glass slide.

Sample	SiO2	TiO2	Al2O3	FeO	MnO	MgO	CaO	Na2O	K2O	P2O5	F	Cl	Total
97-shard-A	40.65	0.02	6.81	0.15	0.04	0.03	0.44	1.21	2.52	0.04	0.48	0.28	52.39
97-shard-A SEM	79.07	0.31	11.66	0.83	0	-0.08	1.16	0.94	6.11				
Glass Slide	74.29	0.03	1.32	0.03	0.02	4.39	6.74	12.14	0.96	0.03	0	0.01	99.95

Table C2: Analyses for the possible shard in PP-612-101 later determined to be a mix of grains.

Sample	SiO2	TiO2	Al2O3	FeO	MnO	MgO	CaO	Na2O	K2O
101-2rd1r	78.69	0.24	8.95	4.98	0.07	2.05	2.43	0.06	2.94
101-2rd1r2	72.27	0.41	11.45	6.42	0.05	2.99	3.2	0.11	2.42
101-2rd1r SEM	74.95		10.3	7.71		3.37	1.44	0	2.22

Table C3: EPMA analyses of GS335 from sample PP-612-48. Conditions: 20 Kv, 5 nA, 3-micrometer beam. Points 7 and 8 use a 10 nA beam.

Sample	SiO2	TiO2	Al2O3	Cr2O3	FeO	MnO	MgO	CaO	Na2O	K2O	P2O5	F	Cl	Total
GS335 SEM	74.59		14.33				0.15		4.21	6.72				
GS335-1	67.31	0.24	14.39	0	1.23	0.12	0.17	0.72	2.47	4.79	0	0.18	0.15	91.78
GS335-2	68.65	0.26	12.97	0.01	1.22	0.09	0.15	0.65	1.93	3.28	0.02	0	0.2	89.46
GS335-4	68.48	0.3	14.66	0	1.31	0.13	0.15	0.68	2.2	4.54	0.07	0.57	0.15	92.96
GS335-5	68.70	0.26	14.38	0.02	1.18	0.1	0.12	0.67	1.9	4.59	0	0	0.14	92.02
GS335-6 qz	98.75	0.03	0	0.04	0.05	0.01	0	0.04	0	0.01	0	0.06	0	99.01
GS335-6 ab	66.22	0	19.86	0	0.03	0	0	0.63	10.93	0.03	0.01	0.17	0.01	97.8
GS335-7 ab	67.67	0	20.29	0	0.03	0	0	0.35	10.72	0.26	0	0	0	99.32
GS335-8 at pt 3	68.79	0.31	14.63	0.01	1.28	0.11	0.12	0.74	0.82	3.93	0.03	0.16	0.15	91.03

Table C4: EPMA analyses for GS335 on 7-3-2013. Conditions: 15kv, 5nA, 3um beam, Na 20 sec peak time.

Sample	SiO2	TiO2	Al2O3	FeO	MnO	MgO	CaO	Na2O	K2O	P2O5	F	Cl	Total
GS335-1	69	0.29	15.22	1.23	0.05	0.15	0.65	4.01	5.94	0.05		0.17	96.65
GS335-2	68.63	0.28	15.89	1.22	0.05	0.15	1.19	4.59	3.93	0.04	0.04	0.14	96.11
GS335-3 ab	68.12		21.63				0.55	11.93	0.08				102.35

Malaysia YTT Analyses

In addition to processing samples from Pinnacle Point, shards from a YTT deposit in Bukit Sap, Malaysia were analyzed. This was done to have a comparison of analyses from the UNLV lab and to also be able to compare how YTT analyses reported in this study match the published data. These shards have bubble-wall morphology and are typically larger than the Pinnacle Point shards. Many of the shards have irregular shapes, and are mostly lacking in vesicles. The deposit this sample comes from is a visible layer only a few hundred kilometers from the Toba caldera. Results are reported in Table C5.

Table C5: Analyses of the Malaysian YTT tephra.

Sample	SiO2	TiO2	Al2O3	Cr2O3	FeO	MnO	MgO	CaO	Na2O	K2O	P2O5	F	Cl	Total
BS1MT1-1	73.41	0.07	12.28	0	0.83	0.07	0.08	0.79	2.85	4.98	0.04	0	0.12	95.5
BS1MT1-2	73.24	0.03	12.15	0	0.81	0.07	0.07	0.76	2.77	4.67	0	0	0.13	94.68
BS1MT1-3	71.59	0.05	11.98	0	0.78	0.07	0.07	0.77	2.7	5.03	0	0	0.12	93.13
BS1MT1-4	73.85	0.04	11.76	0.02	0.88	0.05	0.05	0.77	2.67	4.81	0.02	0.04	0.16	95.05
BS1MT1-5	74.06	0.04	12.31	0.01	0.88	0.08	0.07	0.75	2.76	4.87	0.05	0.57	0.13	96.32
BS1MT1-12	74.11	0.09	11.85	0.03	0.78	0.05	0.03	0.59	2.82	4.89	0.07	0.39	0.14	95.65
BS1MT1-13	74.12	0.05	11.95	0.02	0.81	0.11	0.05	0.7	2.82	4.81	0.04	0	0.15	95.58
BS1MT1-14	74.08	0.06	11.93	0.01	0.85	0.11	0.08	0.79	2.79	4.95	0	0.16	0.16	95.87
BS1MT1-15	73.46	0.05	11.82	0	0.82	0.07	0.04	0.66	2.89	4.71	0.12	0	0.15	94.76
BS1MT1-16	74.04	0	11.97	0	0.76	0.06	0.02	0.55	2.81	4.75	0	0.16	0.18	95.19
BS1MT1-17	74.35	0.02	11.88	0.01	0.81	0.07	0.07	0.8	2.8	4.58	0.02	0.49	0.14	95.8
BS1MT1-18	74.04	0.06	12.27	0	0.85	0.07	0.08	0.78	2.77	5.04	0.05	0	0.13	96.1
BS1MT1-19	74.74	0.01	12.19	0.02	0.81	0.04	0.03	0.69	2.85	4.74	0	0.06	0.17	96.29
BS1MT1-20	73.55	0	11.57	0.02	0.78	0.06	0.04	0.73	2.64	4.97	0.04	0.42	0.15	94.75
BS1MT1-21	73.77	0.07	11.93	0	0.81	0.09	0.06	0.7	2.73	4.74	0	0	0.15	94.99
BS1MT1-22	74.06	0.02	12.14	0	0.78	0.05	0.02	0.72	2.7	4.83	0	0.39	0.14	95.65
BS1MT1-23	74.1	0.01	11.84	0.01	0.73	0.08	0.05	0.76	2.4	4.51	0	0.06	0.16	94.65
BS1MT1-24	74.07	0.06	12.33	0	0.9	0.05	0.06	0.86	2.84	4.88	0	0	0.15	96.16
BS1MT1-26	74.07	0.07	11.68	0	0.8	0.07	0.04	0.66	3.01	4.22	0.04	0.3	0.15	94.94
BS1MT1-27	74.38	0.01	12.08	0	0.89	0.05	0.05	0.8	2.88	4.77	0	0	0.13	96
BS1MT1-28	74.23	0.06	12.17	0.01	0.88	0.05	0.09	0.78	2.73	4.61	0	0.12	0.15	95.81
BS1MT1-29	73.43	0.06	11.97	0	0.91	0.04	0.03	0.84	2.84	4.57	0.06	0.18	0.14	94.97
BS1MT1-30	74.89	0.04	12.08	0.01	0.77	0.07	0.03	0.64	2.96	4.97	0.03	0.1	0.17	96.68
BS1MT1-31	74.05	0.04	12.06	0	0.87	0.06	0.03	0.79	2.87	4.64	0.02	0.22	0.12	95.65
BS1MT1-32	73.95	0.05	12.22	0.02	0.89	0.07	0.08	0.79	2.86	4.98	0.05	0	0.13	96.05
BS1MT1-34	74.06	0.06	11.83	0.04	0.76	0.05	0.04	0.7	2.66	5	0	0	0.13	95.3
BS1MT1-35	73.92	0.04	12.01	0	0.83	0.06	0.05	0.73	2.69	5.05	0.06	0.18	0.12	95.64
BS1MT1-36	74.47	0.04	12.08	0	0.87	0.05	0.05	0.76	2.84	4.94	0.02	0.28	0.14	96.39

Biogenic Silica

Other optically isotropic material was found in the reference slides that have a similar density as the Pinnacle Point shards. These grains were identified as opaline material, phytoliths (Figure C1), and sponge spicules (Figure C2). All are forms of amorphous silica, which means they are isotropic in cross polarized light.

Phytoliths

Phytoliths are grains of SiO_2 formed in plant roots that survive in the sediment after the plant decays. Phytoliths shape is characteristic of a particular plant species (Piperno, 2006). In PP5-6 samples the phytoliths typically have an "etched" appearance. Phytoliths are easy to identify under the microscope because they very high relief, pitted surfaces and distinctive shapes (Piperno, 2006). High SiO_2 and minor amounts of Na_2O and K_2O characterize their major element chemistry. Analytical totals range from 88.27 to 91.36 wt. % (Table C6).

Table C6: EPMA analyses of phytoliths.

Sample	SiO2	Al2O3	TiO2	FeO	MgO	MnO	CaO	Na2O	K2O	P2O5	Cl	F	Total
115-1	89.3	0	0	0	0.08	0.02	0.04	0.71	0.42	0.05	0.14	0.6	91.36
115-2	89.18	0	0	0	0	0.01	0.02	0.75	0.52	0.04	0.17	0	90.69
115-3	86.42	0	0	0	0.01	0.02	0.06	0.64	0.36	0	0.68	0.08	88.27

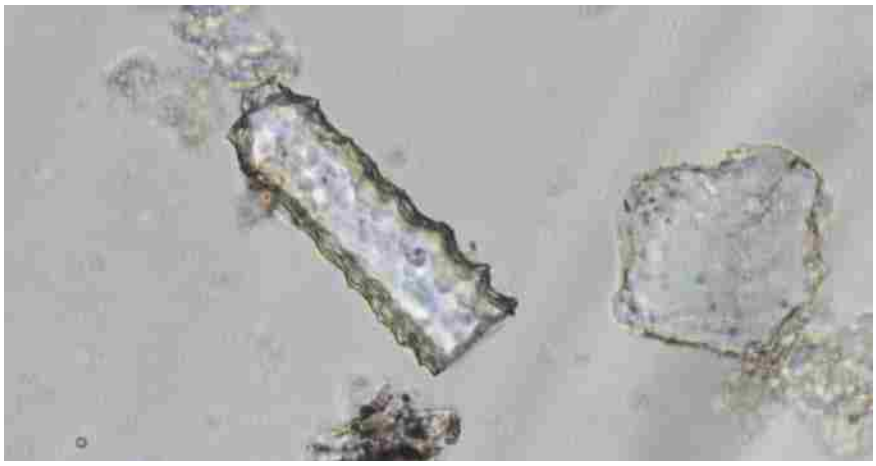

Figure C1: Image of a phytolith under plane polarized light.

Figure C2: Image of a sponge spicule under plane polarized light.

Opaline Material

For this study, opaline material refers to material with opal-like chemistry that are not phytoliths or sponge spicules. The opaline material is isotropic under cross-polarized light and is either clear or light brown in plane-polarized light. It exhibits conchoidal fracture and has cuspate margins that are usually typical of glass shards. Some of the grains also appear to have vesicles and there are instances of slight birefringence around the rims of some of the grains.

Totals for the opaline material ranged from 83.7 to 89.14 wt. %. The grains contain mostly SiO_2 with Al_2O_3 and Na_2O being the two other major elements with concentrations above one weight percent (Table C7). The opaline material is much more abundant in the samples than the cryptotephra.

The opaline material has also been found in larger sieve size fractions as well as in the stratigraphic aggregate below the ALBS; the LBSR (Figure 4). Additionally, it was identified in samples from sand dunes outside of the rock shelter, beach deposits just to the east of PP5-6 and in the sand bag material used to cover the excavation sites. When polished for analysis, the material provides a smooth surface, unlike phytoliths, which have a tendency to crumble.

Table C7: EPMA analyses of opaline material.

Sample	SiO2	TiO2	Al2O3	FeO	MgO	MnO	CaO	Na2O	K2O	P2O5	Cl	F	Total
25-1	78.7	0.05	2.48	0.06	0	0	0.04	4.19	0.05	0	0.11	0.24	85.92
25-2	79.36	0.01	0.36	0.02	0.03	0	0.03	4.02	0.03	0.12	0	0.12	84.1
49-1	85.85	0.15	0.01	0	0.03	0.01	0.07	0.73	0.43	0.02	0.06	0.02	87.38
83-1	79.61	0.02	2.37	0.09	0	0	0.05	3.85	0.05	0	0.06	0	86.1
84-1	80.69	0.01	3.27	0.05	0.03	0.03	0.06	3.55	0.05	0.17	0.07	0	87.98
84-2	80.41	0.03	2.3	0.03	0.03	0.03	0	2.02	0.02	0.14	0.09	0	85.1
85-1	80.45	0	2.37	0	0.03	0.02	0.04	3.42	0.03	0	0.09	0	86.45
85-2	79.67	0	2.5	0.08	0.04	0	0.02	3.96	0.04	0.07	0	0	86.38
85-3	79.4	0.06	2.41	0.04	0	0.04	0	3.87	0.04	0.7	0	0	86.56
100-1	85.69	0.09	1.22	0.63	0.08	0.02	0.41	0.46	0.2	0	0.17	0.03	89
100-2	85.36	0.11	1.42	0.61	0.1	0.02	0.5	0.3	0.26	0.09	0.19	0.18	89.14
100-3	81.52	0.09	1.13	1.01	0.34	0.15	1.31	0.4	0.28	0	1.22	0.13	87.58
105-1	82.19	0	1.14	1.13	0.46	0.013	1.21	2.23	0.72	0.14	2.7	0	91.933
115-1	79.87	0.03	2.27	0.07	0.01	0.04	0.08	3.67	0.08	0.04	0.1	0.4	86.66
115-2	82.84	0.07	1.7	0.32	0.25	0.01	0.71	0.22	0.51	0.01	0.05	0	86.69
115-3	81.94	0.03	0.03	0.14	0.18	0.06	0.52	0.35	0.24	0	0.12	0	83.61
128-1	77.8	0.02	2.36	0.02	0	0	0.05	4.05	0.06	0	0.113	0.03	84.503
128-2	78.88	0	2.34	0	0.02	0	0.04	2.13	0.05	0	0.108	0.15	83.718

Table C8: Normalized values of opaline material versus borosilicate glass without the boron content.

Sample	SiO2	TiO2	Al2O3	FeO	MgO	MnO	CaO	Na2O	K2O	P2O5	Cl	F	Total
25-1	91.60	0.06	2.89	0.07	0	0	0.05	4.88	0.06	0	0.13	0.28	100
25-2	94.36	0.01	0.43	0.02	0.04	0	0.04	4.78	0.04	0.14	0	0.14	100
49-1	98.25	0.17	0.01	0	0.03	0.01	0.08	0.84	0.49	0.02	0.07	0.02	100
83-1	92.46	0.02	2.75	0.10	0	0	0.06	4.47	0.06	0	0.07	0	100
84-1	91.71	0.01	3.72	0.06	0.03	0.03	0.07	4.04	0.06	0.19	0.08	0	100
84-2	94.49	0.04	2.70	0.04	0.04	0.04	0	2.37	0.02	0.16	0.11	0	100
85-1	93.06	0	2.74	0	0.03	0.02	0.05	3.96	0.03	0	0.1	0	100
85-2	92.23	0	2.89	0.09	0.05	0	0.02	4.58	0.05	0.08	0	0	100
85-3	91.73	0.07	2.78	0.05	0	0.05	0	4.47	0.05	0.81	0	0	100
100-1	96.28	0.10	1.37	0.71	0.09	0.02	0.46	0.52	0.22	0	0.19	0.03	100
100-2	95.76	0.12	1.59	0.68	0.11	0.02	0.56	0.34	0.29	0.10	0.21	0.2	100
100-3	93.08	0.10	1.29	1.15	0.39	0.17	1.50	0.46	0.32	0	1.39	0.15	100
105-1	89.40	0	1.24	1.23	0.50	0.01	1.32	2.43	0.78	0.15	2.94	0	100
115-1	92.16	0.03	2.62	0.08	0.01	0.05	0.09	4.23	0.09	0.05	0.12	0.46	100
115-2	95.56	0.08	1.96	0.37	0.29	0.01	0.82	0.25	0.59	0.01	0.06	0	100
115-3	98.00	0.04	0.04	0.17	0.22	0.07	0.62	0.42	0.29	0	0.14	0	100
128-1	92.07	0.02	2.79	0.02	0	0	0.06	4.79	0.07	0	0.13	0.04	100
128-2	94.22	0	2.80	0	0.02	0	0.05	2.54	0.06	0	0.13	0.18	100
BoroGls-1	92.52	0.05	2.66	0.07	0.02	0.01	0.01	4.58	0	0	0	0.08	100
BoroGls-2	92.67	0	2.68	0	0.02	0.01	0	4.37	0.03	0	0.16	0.07	100
BoroGls-3	93.22	0.04	2.64	0	0	0	0.03	3.99	0.02	0	0	0.06	100
BoroGls-4	92.58	0.09	2.65	0.03	0.02	0	0.02	4.48	0	0	0	0.06	100
BoroGls-5	92.3	0	2.68	0.05	0	0.01	0.03	4.69	0.03	0.01	0.12	0.07	100
BoroGls-6	91.68	0	2.76	0.08	0.01	0.03	0.06	4.86	0.02	0	0.39	0.06	100
BoroGls-7	91.71	0	2.84	0.05	0	0	0.02	5.2	0	0	0.13	0.06	100
BoroGls-8	92.44	0	2.65	0	0.03	0	0.04	4.6	0.01	0	0.09	0.15	100
BoroGls-9	92.09	0.03	2.74	0	0	0.02	0.04	4.92	0.04	0	0.03	0.09	100
BoroGls-10	92.28	0	2.67	0.05	0.02	0	0.06	4.72	0.02	0	0.12	0.07	100

APPENDIX D: EXTENDED INTERPRETATIONS

Toba Background

The Toba caldera in Sumatra, Indonesia is 8965 km from Pinnacle Point. Its latest largest eruption was the VEI, Volcano Explosivity Index, 8.8 eruption of the YTT, 73.88 +/- 0.32 ka (Storey et al., 2012). Eruptions with a VEI of 8 or above are considered super-eruptions. Cryptotephra has been shown to travel 7000 km even from small eruptions (Pyne-O'Donnell et al., 2012). The Toba caldera (Lake Toba), 100 x 30 km, in Sumatra, Indonesia is considered to be the largest caldera formed during the Pleistocene (Lane et al., 2011; Chesner, 2012; Williams, 2012). Lengthwise, it is parallel to both the Sumatra Fault zone and Java subduction zone (Williams, 2012). It lies in one of the most seismically active areas in the world and near the site of the 2004 earthquake and Indian Ocean tsunami (Williams, 2012).

Deposits of the YTT (Figure D1) cover India, part of the Indian Ocean, the South China Sea, Bay of Bengal, and East Africa (Williams, 2012). The closest known deposit of the YTT to Pinnacle Point is in Lake Malawi, eastern Africa. This is the most distal documented YTT to date.

Deposits from the 73.88 +/- 0.32 ka Toba super-eruption are called YTT because there are several other, older Toba pyroclastic eruptions: Middle Toba Tuff (MTT) at 501 ka, and Oldest Toba Tuff (OTT) 840 ka (Diehl et al., 1987; Chesner et al., 1991; Chesner, 2012). The MTT was a relatively small eruption compared to the YTT and OTT with a DRE of about 60 km^3. The OTT by comparison was much larger, with a DRE of about 2300 km^3 (Pattan et al., 2010).

Finding biotite is one of the distinguishing characteristics of the YTT (to separate it from the OTT in distal deposits in India and Malaysia) (Smith et al., 2011). In the India ash samples, biotite crystals may be only 5 to 10 micrometers in length (Smith et al., 2011). They would have to be even smaller to make it to South Africa because biotite has a high density, which means that any ash particles that contain

biotite microlites would be deposited closer to the source than those without any mineral phases. Biotite was not found in the Lake Malawi cryptotephra (Chorn, 2012, Lane et al., 2013). Hence, it would not be expected in the Pinnacle Point deposits (assuming the shards are from the YTT).

The YTT eruption was dacitic to rhyolitic in composition with silica ranging from 68 to 77 wt. % (Chesner 2012) but only the most silicic components form distal deposits and the geochemistry should remain uniform (Lane et al., 2013). The dacitic end-member is only found within the Toba caldera (Chesner, 2012). To reach the western coast of Africa, YTT ash would have to traverse the Indian Ocean by either aeolian or sea transport (as rafted pumice). The discovery of the YTT in eastern Africa (Chorn, 2012; Lane et al., 2013) shows that transport of ash from Sumatra to eastern central Africa is possible. However, it would be harder for ash to travel to South Africa.

Opaline Material

The opaline material found in the samples was originally thought to be volcanic shards but microprobe analyses proved otherwise. This material typically shows cuspate margins and appears to have vesicles. A study illustrating the similarities between the appearance of tephra and biogenic silica is Visser (2011). Because of the look and isotropic natural of these opaline grains, they were counted as shards in the early portion of the work for this thesis. This resulted in a frequency profile with shard peaks in the tens of grains and a pattern of two peaks (Smith et al., 2014). After the initial discovery of the opaline material, EPMA analyses were the only way to accurately distinguish the shards from the opaline material (Table C7). Differentiations can now be mostly made using the petrographic microscope but it requires a more meticulous scanning of the reference slides than typical.

The chemistry of the opaline material is distinct from both the Pinnacle Point shards and phytoliths. Phytoliths are mostly silica with a very minor percentage of other elements. The opaline material typically has 2 wt. % Al_2O_3 or more and Na_2O of about 4 wt. % (Table C7). There are several

exceptions to this, however. The percentages of these elements are too much for the opaline material to be considered phytoliths unless they have undergone chemical alteration. The totals are too high to be accounted for simply by an unpolished surface, especially when other grains in the same mount have acceptable totals. Several possible origins were researched for the opaline material: altered tephra, micro-tektites, sinter/geyserite, borosilicate glass contamination, and silcrete.

The low totals of the opal-like analyses infer at least 10 percent LOI (Loss On Ignition), which may be either water or a light element like Boron. The high LOI was used to classify the material as opal. However, Opal-CT has less aluminum and other metals and is not isotropic. The presence of the "extra elements" and the correspondence of one of our collaborators led us to believe the material may be altered glass shards. This would explain why the opaline grains are visually very similar to each other. However, if the opaline material is altered tephra, what caused the alteration? The Pinnacle Point shards themselves do not appear to have any physical signs of alteration or weathering.

Opal A (amorphous opal) occurs in Zone 1 of tephra alteration (Iijima 1988). The opaline material found at Pinnacle Point is found throughout the units in the rock shelter as well as sand bag fill from a nearby quarry and active sand dune and beach material outside the rock shelter. Because of the widespread nature of the opaline material, it is unlikely that is altered tephra. The opaline material appears to be a part of the host sediment of the dunes that make up the majority of the deposits at PP5-6. In this case, the opaline material is a pervasive 'contaminant' that is completely unrelated to the Pinnacle Point shards.

It is possible that the opaline material could be micro-tektites. However, this origin has the same issue as the altered tephra hypothesis due to the amount found in the rock shelter. Micro-tektites are also usually aerodynamically shaped (Koeberl, 1986) while many of the opaline grains have an irregular morphology.

Sinter or geyserite is another possible source of the opaline material. However, this hypothesis is hard to verify because geysers present at 75 ka are likely gone now and the deposits covered. Many of the hot springs near Pinnacle Point have travertine deposits, not sinter (Smith, personal communication 2014).

The opaline material strongly resembles the composition of borosilicate glass (without the boron content). The microprobe at UNLV cannot accurately analyze for boron. Attempts were made to detect the presence of boron in both the opaline material and borosilicate glass using EPMA without obtaining a wt. percentage but the results were inconclusive. Table C8 illustrates the similarities between normalized opaline data and normalized borosilicate glass as it would appear by EPMA analyses. Boron accounts for about 13 wt. % of borosilicate glass. Although chemically a possibility, the morphology of the opaline material does not match that of borosilicate glass shards. Man-made glass fractures with cuspate margins but should not have apparent vesicles.

The opaline material appears to be more prevalent in layers with abundant phytoliths and presumed human activity. In the ALBS and even more so in the SADBS, early humans were utilizing silcrete for tools (Brown et al., 2012). It is possible that the opaline grains are micro-flakes of silcrete that were removed during shaping of the stone tools. They are many outcrops of silcrete present in South Africa (Figure D3) and nearby samples appear geochemically homogeneous throughout an outcrop (Nash et al., 2013). The flaking of stone tools would account for the presence of the material within archaeological deposits but would not explain its presence in the sand dune material or sand quarry.

Based on the available data, no origin or source for the opaline material can be determined at this time. More work is needed to answer questions about the significance of the opaline component

found at Pinnacle Point. Its presence in PP5-6 sediment as well as sandbags and beach sand suggest that this component is ubiquitous in the environment, but its origin is still a mystery.

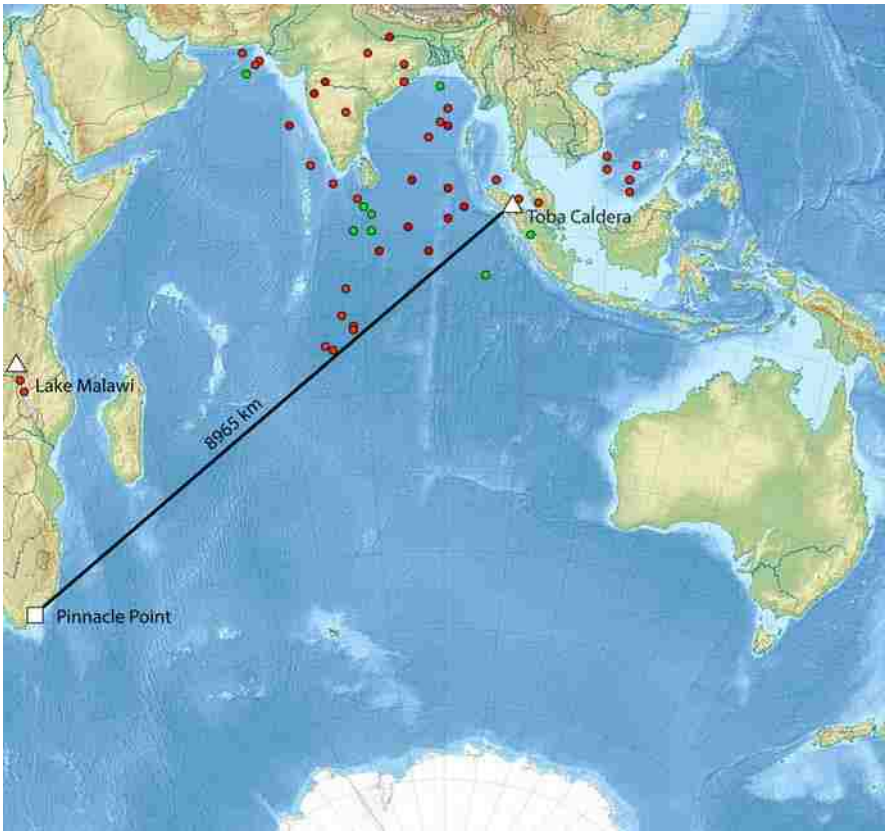

Figure D1: YTT distal deposit location map including the distance between Pinnacle Point and the Toba Caldera.

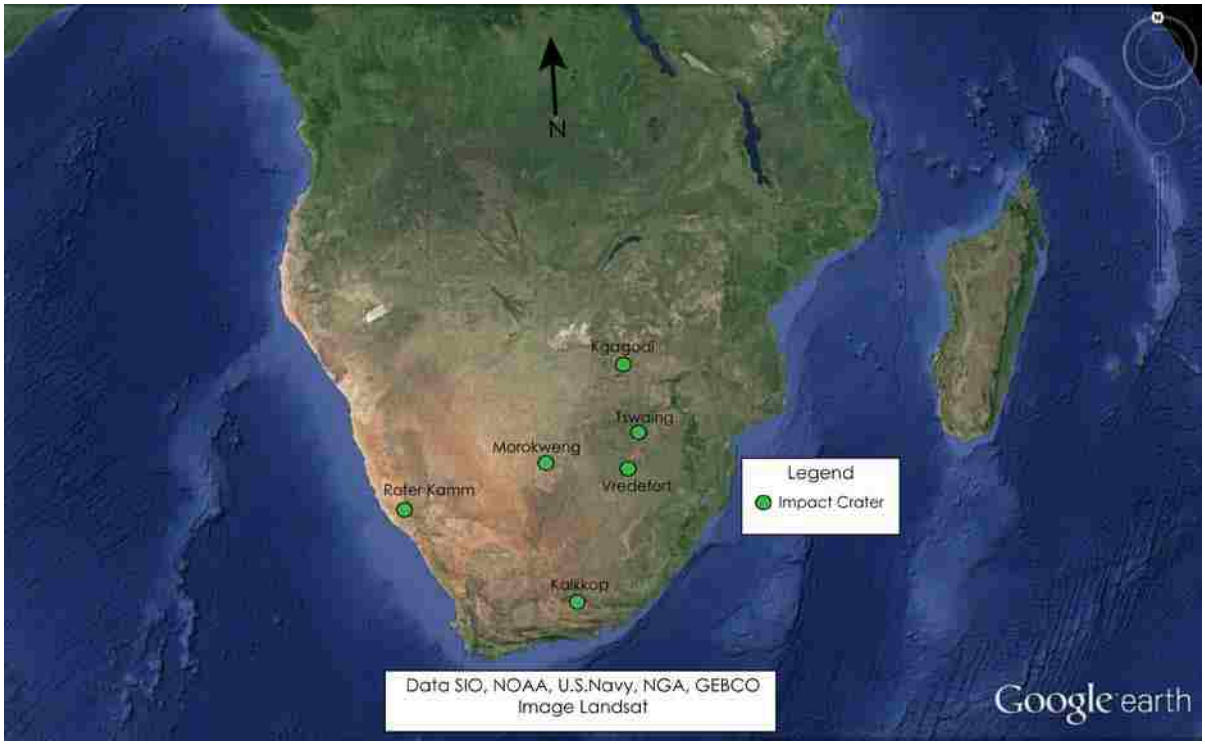

Figure D2: Map of southern Africa impact structures. Impact location data is from Earth Impact Database.

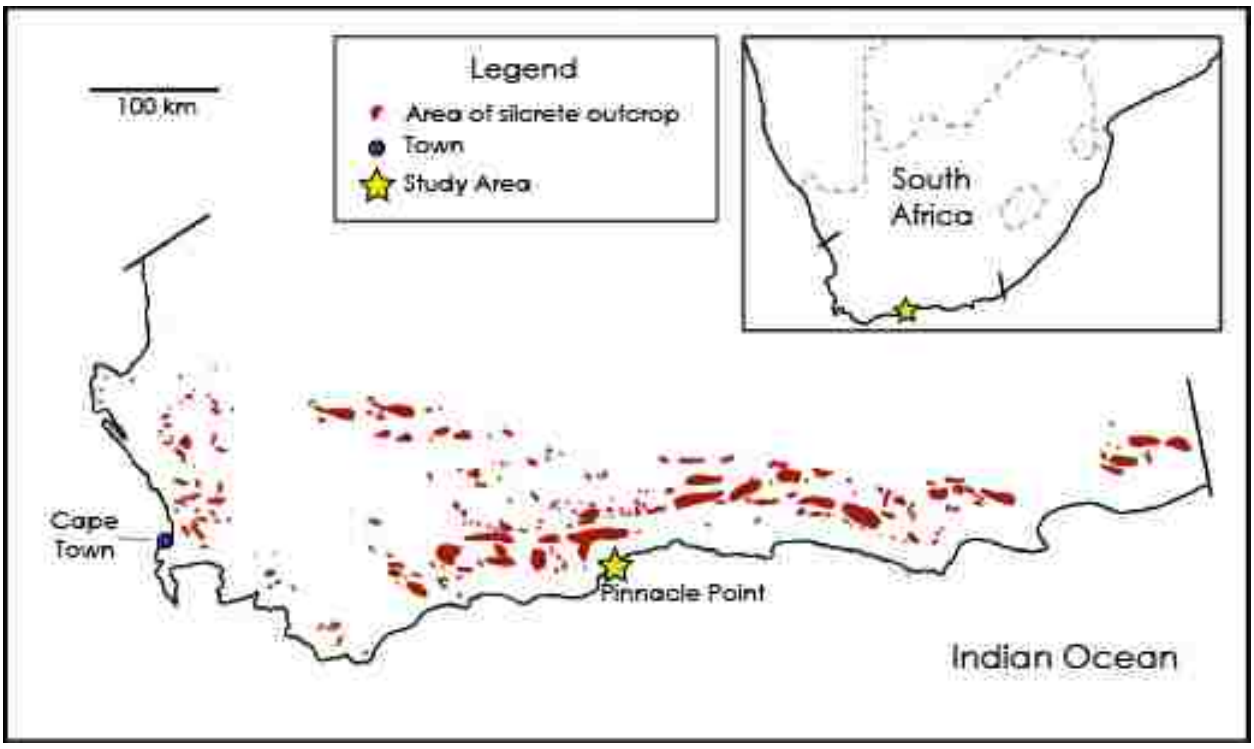

Figure D3: Generalized map of silcrete outcrops in South Africa. Figure modified from Nash et al. (2013)

REFERENCES

Baadsgaard, H., Dodson, M.H., 1964, Potassium—argon ages of sedimentary and pyroclastic rocks: Geological Society London, Special Publications, v. 1, p. 119-127.

Balascio, N.L., Wickler, S., Narmo, L.E., Bradley, R.S., 2011, Distal cryptotephra found in a Viking boathouse: the potential for tephrochronology in reconstructing the Iron Age in Norway: Journal of Archaeological Science, v. 38, p. 934-941.

Bar-Matthews, M., Marean, C.W., Jacobs, Z., Karkanas, P., Fisher, E.C., Herries, A.I.R., Brown, K., Williams, H.M., Bernatchez, J., Ayalon, A., Nilssen, P.J., 2010, A high resolution and continuous isotopic speleothem record of paleoclimate and paleoenvironment from 90 to 53 ka from Pinnacle Point on the south coast of South Africa: Quaternary Science Reviews, v. 29, p. 2131-2145.

Barton, R.N.E, Lane, C.S., Albert, P.G., White, D., Collcut, S.N., Bouzouggar, A., Ditchfield, P., Farr, L., Oh, A., Ottolini, L., Smith, V.C., Van Peer, P., Kindermann, K., 2015, The role of cryptotephra in refining the chronology of Late Pleistocene human evolution and cultural change in North Africa: Quaternary Science Reviews, v. 118, p. 151-169.

Bernatchez, J.A., Marean, C.W., 2011, Total Station Archaeology and the Use of Digital Photography: The SAA Archaeological Record, v. 77, p.16-21.

Blegen, N., Tryon, C.A., Faith, J.T., Peppe, D.J., Beverly, E.J., Li, B., Jacobs, Z., 2015, Distal tephras of the eastern Lake Victoria basin, equatorial East Africa: correlations, chronology and a context for early modern humans: Quaternary Science Reviews, v. 122, p. 89-111.

Blockley, S.P.E., Pyne-O'Donnell, S.D.F., Lowe; J.J., Matthews, I.P., Stone A., Pollard, A.M., Turney, Molyneux, E.G., 2005, A new and less destructive laboratory procedure for the physical separation of distal glass tephra shards from sediment: Quaternary Science Reviews, v. 24, p. 1952-1960.

Blockley, S.P.E., Bronk Ramsey, C., Highman, T.F.G., 2008. The Middle to Upper Paleolithic Transition: dating, stratigraphy, and isochronous markers: Journal of Human Evolution, v. 55 (5), p. 764-771.

Branch, N., Canti, M., Clark, P., Turney, C., 2014, Environmental Archaeology: Theoretical and practical approaches: New York, Oxford University Press, 240 p.

Brown, F.H., Haileab, B., McDougall, I., 2006, Sequence of tuffs between the KBS Tuff and the Chari Tuff in the Turkana Basin, Kenya and Ethiopia: Journal of the Geological Society of London, v. 163, p. 185-204.

Brown, K.S., Marean, C.W., Herries, A.I.R., Jacobs, Z., Tribolo, C., et al., 2009, Fire as an Engineering Tool of Early Modern Humans: Science, v. 325, p. 859-862.

Brown, K.S., Marean, C.W., Jacobs, Z., Schoville, B.J., Oestmo, S., et al., 2012, An early and enduring advanced technology originating 71,000 years ago in South Africa: Nature, v. 491, p. 590-593.

Chesner, C.A., Rose, W.I., Deino, A., Drake, R., 1991, Eruptive history of Earth's largest Quaternary caldera (Toba, Indonesia) clarified: Geology, v. 19, p. 200-203.

Chesner, C.A., 2012, The Toba Caldera Complex: Quaternary International, v. 258, p. 5-18.

Chorn, B., 2012, Tephrochronology of the Lake Malawi Drill Cores: A Feasibility Study. [Master of Science]: University of Minnesota, 119 p.

Davies, S.M., 2015, Cryptotephras: the revolution in correlation and precision dating: Journal of Quaternary Science, v. 30, p. 114-30.

Dehn, J., Farrell, J.W., Schmincke, H.-U., 1991. Neogene tephrochronology from Site 758 on northern Ninetyeast Ridge: Indonesian arc volcanism of the past 5 ma: Proceedings Ocean Drilling Program, Scientific Results, v. 121, p. 273-295.

D'Errico, F., and Henshilwood, C.S., 2007, Additional evidence for bone technology in the southern African Middle Stone Age: Journal of Human Evolution, v. 52, p.142-163.

Dibble, H., Marean, C.W., McPherron, S.P., 2007, The use of barcodes in excavation projects: SAA Archaeological Record, v. 7, p. 33-38.

Diehl, J.F., Onstott, T.C., Chesner, C.A., Knight, M.D., 1987. No short reversals of Brunhes age recorded in the Toba tuffs, north Sumatra, Indonesia: Geophysical Research Letters, v. 14, p. 753-756.

Dugmore, A.J., Larsen, G., Newton, A.J., Sugden, D.E., 1992, Geochemical stability of fine-grained silicic Holocene tephra in Iceland and Scotland: Journal of Quaternary Science, v. 7, p. 173–183.

Dunbar, N.W., Kurbatov, A.V., 2011, Tephrochronology of the Siple Dome ice core, West Antarctica: correlations and sources: Quaternary Science Reviews, v. 30, p. 1602-1614.

Feakins, S.J., Brown, F.H., deMenocal, P.B., 2007, Plio-Pleistocene microtephra in DSDP site 231, Gulf of 375 Aden: Journal of African Earth Sciences, v. 48, p. 341-352.

Fisher, E.C., Akkaynak, D., Harris, J., Herries, A.I.R., Jacobs, Z., et al., 2015, Technical considerations and methodology for creating high-resolution, color-corrected, and georectified photomosaics of stratigraphic sections at archaeological sites: Journal of Archaeological Science, v. 57, p. 380-394.

Fisher, E.C., Bar-Matthews, M., Jerardino, A., Marean, C.W., 2010, Middle and Late Pleistocene Paleoscape Modeling along the Southern Coast of South Africa: Quaternary Science Reviews, v. 29, p. 1382-1398.

Fisher, R.V., and Schmincke, H-U., 1984, Pyroclastic Rocks: Berlin, New York, Springer-Verlag, 472 p.

Fontijn K, Ernst GGJ, Elburg MA, Williamson D, Abdallah E, et al., 2010, Holocene explosive eruptions in the Rungwe Volcanic Province, Tanzania: Journal of Volcanology and Geothermal Research, v. 196, p. 91-110.

Fontijn, K., Elburg M.A., Nikogosian, I.K., van Bergen, M.J., Ernst, G.G.J., 2013, Petrology and geochemistry of Late Holocene felsic magmas from Rungwe volcano (Tanzania), with implications for trachytic Rungwe Pumice eruption dynamics: Lithos, v. 177, p. 34-53.

Gatti, E., Mokhtar, S., Talib, K., Rashidi, N., Gibbard, P., Oppenheimer, C., 2013, Depositional processes of reworked tephra from the Late Pleistocene Youngest Toba Tuff deposits in the Lenggong Valley, Malaysia: Quaternary Research, v. 79, p. 228-241.

Gatti, E., Villa, I.M., Achyuthan, H., Gibbard, P.L., Oppenheimer, C., 2014, Geochemical variability in distal and proximal glass from the Youngest Toba Tuff eruption: Bulletin of Volcanology, v. 76, p. 859-875.

Gehrels, M.J., Newnham, R.M., Lowe, D.J., Wynne, S., Hazell, Z.J., Caseldine, C., 2008, Towards rapid assay of cryptotephra in peat cores: Review and evaluation of various methods: Quaternary International, v. 178, p. 68-84.

Haileab, B., 1995, Geochemistry, geochronology and tephrostratigraphy of tephra from the Turkana Basin, southern Ethiopia and Northern Kenya [Ph.D. dissertation]: University of Utah, pp. 369.

Henshiwood, C.S., 2008, Winds of change: Palaeoenvironments, materials, culture and human behavior in the late Pleistocene (~77 ka-48 ka ago) in the Western Cape Province, South Africa: South African Geological Society, Goodwin Series, v. 10, p. 35-51.

Housley, R.A., MacLeod, A., Armitage, S.J., Kabaciński, J., Gamble, C.S., 2014, The potential of cryptotephra and OSL dating for refining the chronology of open-air archaeological windblown sand sites: A case study from Mirkowice 33, northwest Poland: Quaternary Geochronology, v.20, p. 99-108.

Iijima, A., 1988, Diagenetic transformations of minerals as exemplified by zeolites and silica minerals; a Japanese view: Developments in Sedimentology, v. 43, p. 147-188.

Jarosewich, E., Nelen, J. A., and Norberg, J. A., 1980a, Reference Samples for Electron Microprobe Analysis: Geostandards Newsletter, v. 4, p. 43-47.

Jarosewich, E., Nelen, J. A., and Norberg, J. A., 1980b, Corrections: Geostandards Newsletter, v. 4, p. 257-258.

Jensen, B.J.L., Pyne-O'Donnell, S., Plunkett, G., Froese, D.G., Hughes, P.D.M., et al., 2014, Transatlantic distribution of the Alaskan White River Ash: Geology, v. 42, p. 875-878.

Jochum, K. P. et al., 2006, MPI-DING reference glasses for in situ microanalysis: New reference values for element concentrations and isotope ratios: Geochemistry, Geophysics, Geosystems, v. **7**, p. 1525-2027.

Karkanas, P., Brown, K.S., Fisher, E.C., Jacobs, Z., Marean, C.W., 2015, Interpreting human behavior from depositional rates and combustion features through the study of sedimentary microfacies at site Pinnacle Point 5-6, South Africa: Journal of Human Evolution, p. 1-21.

Karkanas, P., Goldberg, P., 2010, Site formation processes at Pinnacle Point Cave 13B (Mossel Bay, Western Cape Province, South Africa): resolving stratigraphic and depositional complexities with micromorphology: Journal of Human Evolution, v. 59, p. 256-73.

Keyser, N., 1997, Geological Map of the Republic of South Africa and the Kingdoms of Lesotho and Swaziland: Council for Geoscience, Pretoria.

Koeberl, C., 1986, Geochemistry of Tektites and Impact Glasses: Annual Review of Earth and Planetary Science, v. 14, p. 323-350.

Lamplugh, G.W., 1902, Calcrete: Geological Magazine, v. 9, p. 75.

Lane, C.S., Chorn, B.T., Johnson, T.C., 2013, Ash from the Toba supereruption in Lake Malawi shows no volcanic winter in East Africa at 75 ka: Proceedings of the National Academy of Sciences, v. 110, p. 8025-8029.

Lane, C.S., Cullen V.L., White D., Bramham-Law C.W.F., Smith V.C., 2014, Cryptotephra as a dating and correlation tool in archaeology: Journal of Archaeological Science, v. 42, p. 42-50.

Lee, S., Bronk Ramsey, C., and Hardiman, M., 2013, Modeling the Age of the Cape Riva (Y-2) Tephra: Radiocarbon, v. 55(2–3), p. 741-747.

Liang, X., Wei, G., Shao, L., Li, X., Wang, R., 2001, Records of Toba eruptions in the South China Sea-Chemical characteristics of the glass shards from ODP 1143A: Science in China (Series D), v. 4, p. 871-878.

Lowe, J.J., Walker, M.J.C., 2014, Reconstructing Quaternary Environments: New York, Routledge (3rd Edition), 472 p.

Lowe, D.J., 2011, Tephrochronology and its application: a review: Quaternary Geochronology, v. 6(2), p. 107-153.

Lowe, J., Barton, N., Blockley, S., Ramsey, C.B., Cullen, V.L., Davies, W., Gamble, C., Grant, K., Hardiman, M., Housley, R., Lane, C.S., Lee, Sharen, Lewis, M., MacLeod, A., Menzies, M., Müller, W., Pollard, M., Price, C., Roberts, A.P., Rohling, E.J., Satow, C., Smith, V.C., Stringer, C.B., Tomlinson, E.L., White, D., Albert, P., Arienzo, I., Barker, G., Borić, D., Carandente, A., Civetta, L., Ferrier, C., Guadelli, J., Karkanas, P., Koumouzelis, M., Müller, U.C., Orsi, G., Pross, J., Rosi, M., Shalamanov-Korobar, L., Sirakov, N., Tzedakis, P.C., 2012, Volcanic ash layers illuminate the resilience of Neanderthals and early modern humans to natural hazards: Proceedings of the National Academy of Sciences, v. 109 (34), p. 13532-13537.

Marean, C.W., Nilssen, P.J., Brown, K., Jerardino, A., Stynder, D., 2004, Paleoanthropological investigations of Middle Stone Age sites at Pinnacle Point, Mossel Bay (South Africa): Archaeology and hominid remains from the 2000 Field Season: Paleoanthropology Abstract.

Marean, C.W., 2010, Pinnacle Point Cave 13B (Western Cape Province, South Africa) in context: The Cape Floral kingdom, shellfish, and modern human origins: Journal of Human Evolution, 59, p. 425-43.

Marean, C.W., Bar-Matthews, M., Fisher, E., Goldberg, P., Herries, A., et al., 2010, The stratigraphy of the Middle Stone Age sediments at Pinnacle Point Cave 13B (Mossel Bay, Western Cape Province, South Africa): Journal of Human Evolution, v. 59, p. 234-255.

Marean, C.W., Cawthra, H.C., Cowling, R.M., Esler, K.J., Fisher, E., et al., 2014, Stone Age People in a Changing South African Greater Cape Floristic Region. *In* Ecology and Evolution of Fynbos: Understanding Megadiversity, N Allsopp, JF Colville, T Verboom, eds.: Oxford, Oxford University Press, pp. 164-99.

Mark, D.F., Petraglia, M., Smith, V.C., Morgan, L.E., Barfod, D.N., Ellis, B.S., Pearce, N.J., Pal, J.N., Korisettar, R., 2014, A high-precision 40Ar/39Ar age for the Young Toba Tuff and dating of ultra-distal tephra: Forcing of Quaternary climate and implications for hominin occupation of India: Quaternary Geochronology Special Issue: Advances in 40Ar/39Ar Dating of Quaternary Events and Processes, v. 21, p. 90-103.

Marshall, A.S., et al., 2009, Fractionation of peralkaline silicic magmas: The greater Olkaria volcanic complex, Kenya Rift Valley: Journal of Petrology, v. 50 (2), p. 323-359.

Mastin, L.G., Guffanti, M., Ewert, J.E., and Spiegel, J., 2009, Preliminary spreadsheet of eruption source parameters for volcanoes of the world: U.S. Geological Survey Open-File Report 2009-1133, v. 1.2, 25 p.

Matthews, N.E., Smith, V.C., Costa, A., Durant, A.J., Pyle, D.M., Pearce, N.J.G., 2012, Ultra-distal tephra deposits from super-eruptions: Examples from Toba, Indonesia and Taupo Volcanic Zone, New Zealand: Quaternary International, v. 258, p. 54-79.

Narcisi B, Petit JR, Delmonte B, Basile-Doelsch I, Maggi V., 2005, Characteristics and sources of tephra layers in the EPICA-Dome C ice record (East Antarctica): implications for past atmospheric circulation and ice core stratigraphic correlations: Earth and Planetary Science Letters, v. 239, p. 253-265.

Nash, D.J., Coulson, S., Staurset, S., Smith, M.P., Ullyott, J.S., 2013, Provenancing silcrete in the Cape coastal zone: implications for Middle Stone Age Research in South Africa: Journal of Human Evolution, v. 65 (5), p. 682-688.

Ninkovich, D., Shackleton, N., Abdel-Monem, A., Obradovich, J., Izett, G., 1978, K-Ar age of the late Pleistocene eruption of Toba, north Sumatra: Nature, v. 276, p. 574-577.

Ninkovich, D., 1979, Distribution, age and chemical composition of tephra layers in deep-sea sediments off western Indonesia: Journal of Volcanology and Geothermal Research, v. 5, p. 67-86

Pattan, J.N., Shane, P., Banaker, V.K., 1999, New occurrence of Youngest Toba Tuff in abyssal sediments of the Central Indian Basin: Marine Geology, v. 155 (3-4), p. 243-248.

Pattan, J.N., Prasad, M.S., Babu, E.V.S.S.K., 2010, Correlation of the oldest Toba Tuff to sediments in the central Indian Ocean Basin: Journal of Earth Systems Science, v. 119, p. 531-539.

Pearce, N.J.G., Abbott, P.M., Martin-Jones, C., 2014, Microbeam methods for the analysis of glass in fine-grained tephra deposits: a SMART perspective on current and future trends, *in* Austin, W.E.N., Abbott, P.M., Davies, S.M., Pearce, N.J.G., Wastegård, S., eds., Marine Tephrochronology, Geological Society of London Special Publication, v. 398, p. 29-46.

Petraglia, M., Korisettar, R., Boivin, N., Clarkson, C., Ditchfield, P., et al., 2007, Middle Paleolithic Assemblages from the Indian Subcontinent Before and After the Toba Super-Eruption: Science, v. 317, p. 114-116.

Petraglia, M.D., Korisettar R., Pal J.N., 2012, The Toba volcanic super-eruption of 74,000 years ago: Climate change, environments, and evolving humans: Quaternary International, v. 258, p. 1-4.

Pilcher, J.R., Hall, V.A., 1992, Towards a tephrochronology for the Holocene of the north of Ireland: The Holocene, v. 2, p. 255–259.

Pilcher, J.R., Hall, V.A., McCormac, F.G., 1995, Dates of Holocene Icelandic volcanic eruptions from tephra layers in Irish peats: The Holocene, v. 5, p. 103-110.

Piperno, Dolores R., 2006, Phytoliths: A Comprehensive Guide for Archaeologists and Paleoecologists: New York, AltaMira Press, 238 p.

Purbo-Hadiwidjoyo, M.M., Sjachrudin, M.L., Suparka, S., 1979, The volcano-tectonic history of the Maninjau caldera, western Sumatra, Indonesia: Geologie en Mijnbouw, v. 58, p. 193-200.

Pyle, D., 1989, The thickness, volume, and grainsize of tephra fall deposits: Bulletin of Volcanology, v, 51, p. 1-15.

Pyne-O'Donnell, S.D.F., 2007, Three new distal tephras in sediments spanning the Last Glacial–Interglacial Transition in Scotland: Journal of Quaternary Science, v. 22, p. 559–570.

Pyne-O'Donnell, S.D.F., Hughes, P.D.M., Froese, D.G., Jensen, B.J.L., Kuehn, S.C., Mallon, G., Amesbury, M.J., Charman, D.J., Daley, T.J., Loader, N.J., Mauquoy, D., Street-Perrott, F.A., Woodman-Ralph, J.,2012, High-precision ultra-distal Holocene tephrochronology in North America: Quaternary Science Reviews, v. 52, p. 6-11.

Schulz, H., Emeis, K.C., Erlenkeuser, H., von Rad, U., Rolf, C., 2002, The Toba volcanic event and interstadial/stadial climates at the marine isotopic stage 5 to 4 transition in the Northern Indian Ocean: Quaternary Research, v. 57 (1), p. 22-31.

Shane, P., Westgate, J., Williams, M., Korisettar, R., 1995, New Geochemical evidence for the Youngest Toba Tuff in India: Quaternary Research, v. 44, p. 200-204.

Smith, E.I., Ciravolo, A., Karkanas, P., Marean, C., Fisher, E., Cleghorn, N., Lane, C., Ren, M., 2014, Cryptotephra Possibly from the 74 ka Eruption of Toba Discovered at Pinnacle Point, South Africa: Implications for Resolving the Dating Controversy for Middle Stone Age Sites in Southern Africa, Paleoanthropology 2014: 23rd Annual Meeting of the Paleoanthropology Society, p. A24.

Smith V.C., Pearce N.J.G., Matthews N.E., Westgate J.A., Petraglia M.D., et al., 2011, Geochemical fingerprinting of the widespread Toba tephra using biotite compositions: Quaternary International, v. 246, p. 97-104.

Stern, C. R., 2004), Active Andean volcanism: its geologic and tectonic setting: Revista geológica de Chile, v. 31 (2), p. 161-206.

Stern, C.R., 2008, Holocene tephrochronology record of large explosive eruptions in the southernmost Patagonian Andes: Bulletin of Volcanology, v. 70, p. 435-454.

Storey M., Roberts R.G., Saidin M., 2012, Astronomically calibrated 40Ar/39Ar age for the Toba supereruption and global synchronization of late Quaternary records: Proceedings of the National Academy of Sciences, v. 109, p. 18684-18688.

Turney, C.S.M., Lowe, J.J., Davies, S.M., Hall, V., Lowe, D.J., Wastegård, S., Hoek, W.Z., Alloway, B., et al., 2004, Tephrochronology of Last Termination Sequences in Europe: a protocol for improved analytical precision and robust correlation procedures (a joint SCOTAV-INIMATE proposal): Journal of Quaternary Science, v. 19 (2), p. 111-120.

Visser, M.P.E., 2012, Detection of middle to late Holocene Icelandic cryptotephras in the Netherlands: tephra versus biogenic silica [Master thesis]: Utrecht, Utrecht University, 26 p.

Wastegård, S., Hall, V.A., Hannon, G.E., van den Bogaard, C., Pilcher, J.R., Sigurgeirsson, M.A., Hermanns-Auoardottir, M., 2003, Rhyolitic tephra horizons in northwestern Europe and Iceland from the AD 700s-800s: a potential alternative for dating first human impact: The Holocene, v. 13 (2), p. 277-283.

Williams M., 2012, The ~73 ka Toba super-eruption and its impact: History of a debate: Quaternary International, v. 258, p. 19-29.

Wulf, S., Kraml, M., Brauer, A., Keller, J., Negendank, J.F.W., 2004, Tephrochronology of the 100 ka lacustrine sediment record of Lago Grande di Monticchio (southern Italy): Quaternary International, v. 122 (1), p. 7-30.

CURRICULUM VITAE

Amber Elizabeth Ciravolo

Department of Geoscience

Mail Stop 4010

University of Nevada Las Vegas

ciravolo@unlv.nevada.edu

a. Professional Preparation

Furman University	Geology, Asian Studies	B.S., 2012
University of Nevada Las Vegas	Geology	M.S., *est. 2015*

b. Appointments

2015 – 2015: Graduate teaching assistant for Igneous and Metamorphic Petrology, Department of Geoscience, University of Nevada, Las Vegas

2013 – 2014: Graduate research assistant for Dr. Eugene Smith, Department of Geoscience, University of Nevada, Las Vegas

2013 – 2015: Lab worker for UNLV Cryptotephra Extraction Lab, Department of Geoscience, University of Nevada, Las Vegas

2012 – 2013: Graduate teaching assistant for Distance Education: Geology 101, Department of Geoscience, University of Nevada Las Vegas

c. Publications (Conference Abstracts)

(i) Most closely related to current project

1. Ciravolo, A.E., Smith, E.I., 2014, Cryptotephra from Archaeological Site at Pinnacle Point, South Africa: Is it from Toba: "Tephra 2014, Maximizing the potential of tephra for multidisciplinary science" *Handbook-Workshop,* 4-8 August 2014, http://www.geohazards.buffalo.edu/documents/Registration.php.

2. Ciravolo, A.E., Smith, E.I., 2013, Origin of Glass Shards from Pinnacle Point, South Africa: Are They from the Super-Eruptions of Toba: "94th Annual Meeting Program with Abstracts" *Proceedings of the American Association for the Advancement of Science Pacific Division* 2013:v32.

3. Ciravolo, A.E., Smith, E.I., 2013, Origin Of Glass Shards From Pinnacle Point, South Africa: Are They From The Super-Eruption Of Toba: "The 8th Annual UNLV Geosymposium, 12 April 2013", pp 28.

4. Smith, E.I., Ciravolo, A., Karkanas, P., Marean, C., Fisher, E., Cleghorn, N., Lane, C., Ren, M., 2014, Cryptotephra Possibly from the 74 ka Eruption of Toba Discovered at Pinnacle Point, South Africa: Implications for Resolving the Dating Controversy for Middle Stone Age Sites in Southern Africa: "Paleoanthropology Society Meeting Abstracts, Calgary, Canada, 8-9 April 2014" *PaleoAnthropology* 2014:A24.

(ii) Other significant publications

1. Ciravolo, A.E., Coulson, A.B., 2012, Comparing the Effects of Transport-Induced Fluvial Abrasion on Avian and Nonavian Vertebrate Skeletal Remains: "GSA Southeastern Section 61st Annual Meeting Abstracts, Asheville, North Carolina, 1-2 April 2012" *GSA Abstracts* 2012.

d. Synergistic Activities

1. Volunteered at Geosymposium, 2013-2015.
2. Archaeological Field Season at Pinnacle Point May-July 2014.
3. Tephra Workshop August 2014.

e. Collaborators & Other Affiliations

(i) Collaborators:

Curtis Marean, Arizona State University; Erich Fischer, Arizona State University; Naomi Cleghorn, University of Texas, Arlington; Zenobia Jacobs, University of Wollagong, Australia; Minghua Ren, University of Nevada, Las Vegas; Christine Lane, University of Manchester.

(ii) Graduate Advisors

Dr. Eugene I Smith (graduate advisor), University of Nevada, Las Vegas